



Rui Filipe de Jesus Cabeça

Licenciatura em Engenharia dos Materiais

Magnetic tweezers for captive disclination loops

Dissertação para obtenção do Grau de Mestre em
Engenharia dos Materiais

Orientadora: Professora Doutora Maria Helena Godinho, Professora
Auxiliar com agregação,
Faculdade de Ciências e Tecnologia da Universidade
Nova de Lisboa

Júri

Presidente: Prof.Doutor João Paulo Borges
Arguente: Prof.João Luis Maia Figueirinhas
Vogal: Prof.Doutora Maria Helena Godinho



FACULDADE DE
CIÊNCIAS E TECNOLOGIA
UNIVERSIDADE NOVA DE LISBOA

March, 2017

Magnetic tweezers for captive disclination loops

Copyright © Rui Filipe de Jesus Cabeça, 2017.

A Faculdade de Ciências e Tecnologia e a Universidade Nova de Lisboa tem o direito, perpétuo e sem limites geográficos, de arquivar e publicar esta dissertação através de exemplares impressos reproduzidos em papel ou de forma digital, ou por qualquer outro meio conhecido ou que venha a ser inventado, e de a divulgar através de repositórios científicos e de admitir a sua cópia e distribuição com objetivos educacionais ou de investigação, não comerciais, desde que seja dado crédito ao autor e editor.

Acknowledgements

Agradeço profundamente à professora Helena Godinho, não só por ter sido a pessoa que me guiou durante todas as etapas deste projecto, mas também por todo o tempo e ajuda que me deu para conseguir finalizar esta dissertação. O compromisso demonstrado pela mesma foi inalcançável. De salientar também o enorme gosto e motivação com que encarou este projecto.

A very special thank you to Professor Pawel Pieranski, who gave me a lot of guidance and help during my stay in France. I'm grateful for all the help given to carrying out the research work, and for all the morning sessions of learning at the cafeteria.

Um agradecimento especial também ao Professor João Canejo, por toda a ajuda prestada no laboratório, e pelo tempo que dispensou para me ajudar. Devo salientar também a simpatia e alegria com que encara o dia-a-dia.

Uma palavra de apreço para a Ana Almeida, também pelo tempo que dispensou para me ajudar nas tarefas de laboratório, e por ter dispensado as folhas das plantas que utilizei neste projecto.

Quero agradecer ao Professor João Paulo Borges, principalmente pela disponibilidade e ajuda constante que me proporcionou durante todo o curso.

Por último, mas não menos importante, agradecer aos meus pais, não só pela ajuda financeira durante todos estes anos, mas também pela motivação e encorajamento que me deram.

It is known that Liquid crystals (LCs) are very sensitive to external fields, making them very desirable regarding technological applications. The uniaxial nematic phase, with long-range orientational order, is widely studied, presenting molecular alignment singularities known as disclination lines. The manipulation of these lines opens new perspectives in the LCs field.

In fact recent studies showed that what appeared to be a point defect in a nematic liquid crystal, are actually nanometer-sized closed-loops[1], that can selectively trigger self-assemble molecular processes.[2]. The disclination loops appearance as well as position, when threaded on polymeric fibers with axial anchoring, can be precisely controlled.

In this work, we present results concerning the generation and precise manipulation these disclination loops, on a micro-scale, threaded on nylon, micro plants cellulose-based filaments and electrospun fibers, immersed in homeotropic nematic cells, with the application of a magnetic field.

Keywords: Nematics, loops, fibers, fields, manipulation, anchoring

É sabido que os Cristais líquidos são muito sensíveis à aplicação de campos externos, tornando-os assim muito desejáveis no que toca a aplicações tecnológicas. A fase nemática uniaxial, com ordem orientacional de longo alcance, está amplamente estudada, apresentando defeitos no alinhamento molecular denominados linhas de disclinação. A manipulação destas linhas abre novas perspectivas no que toca ao ramo dos cristais líquidos.

Estudos recentes mostram que o que aparenta ser um defeito pontual num cristais líquido nemático, são na realidade anéis de disclinação, à escala nanométrica[1], e estes podem desencadear processos de ordenamento molecular de forma bastante selectiva[2]. O aparecimento destas linhas de disclinação, bem como a sua posição, quando estão enroladas à volta de fibras poliméricas com ancoragem planar, são condições que podem ser facilmente controladas.

Neste trabalho, apresentamos resultados tendo em conta a geração e manipulação precisas destes anéis, à escala micrométrica, quando enrolados em fibras de nylon, em micro filamentos de plantas à base de celulose e fibras de electrospinning, quando inseridas em células nemáticas com ancoragem homeotrópica, recorrendo à aplicação de campos magnéticos.

Palavras-chave: Nemáticos, anéis, fibras, campos, manipulação, ancoragem

Abbreviations

LC(s)	Liquid Crystals
POM	Polarized optical microscope
HPC	Hydroxypropylcellulose
5CB	4'-n-pentyl-4-cyanobiphenyl
EN18	Nematic liquid crystal mixture ($\Delta_\xi < 0$)
CCD	Charge-coupled device
CA	Cellulose acetate
DMac	Dimethylacetamide
AC	Alternating current

B	Magnetic field
C_g	Chirogyral coefficient
d	Sample thickness
Δ_χ	Diamagnetic anisotropy
f	Resulting force per unit length
F	Elastic energy per unit surface
f_d	Frank's free energy
f_l	Laplace force
f_r	Laplace opposite force
h	Distance between the fiber and the disclination
K	Frank elastic constant
K_{11}	Splay elastic constant
K_{22}	Twist elastic constant
K_{33}	Bend elastic constant
M	Magnetization
m	Topological charge
m	Molecule's magnetization
\overline{M}_n	Average number molecular weight
Γ_M	Magnetic torque
n	Director
R	Fiber's radius
S	Order parameter
T	Temperature
T_e	Disclination line tension
t	Time
τ	Time constant
$\xi(B)$	Magnetic coherence length
w/w	Weight per weight

Abbreviations	xi
Symbols	xiii
List of Figures	xvi
1 Introduction	1
1.1 Aims of the present work	1
1.2 Liquid Crystals: Nematic Phase	1
1.2.1 Frank’s continuous elastic theory	2
1.2.2 Surface Anchoring	3
1.2.3 Topological Defects	3
1.2.4 Captive disclination loops on fibers	5
1.2.5 External Fields	5
2 Experimental and Characterization Techniques	7
3 Results and Discussion	9
3.1 Planar Axial Anchoring	9
3.2 Tilted magnetic field, translation of disclination loops	10
3.3 Trap-like action of an inhomogeneous magnetic field	12
3.4 Captive disclination loops, the chirogyral effect	13
3.5 Generation of captive disclination loops by electrohydrodynamic turbulence	14
3.6 Magnetic Traps	16
3.7 Field induced translation of disclination loops	20
3.8 Horizontal magnetic fields on CA electrospinning fibers	22
3.9 Horizontal magnetic fields on natural fibers	26
4 Conclusions and Future Perspectives	29
Bibliography	30
A Appendix	33

1.1	a) POM picture of the nematic phase, between cross-polarizers; b) Schematic representation of the director \vec{n} , showing the average orientation of the calamitic molecules, and θ , the deviation between an arbitrary nematic calamitic molecule and the director \vec{n}	2
1.2	Schematic representation of the different types of elastic deformations in nematic liquid crystal: a) Splay (K_{11}); b) Twist (K_{22}); c) Bend (K_{33})[9].	3
1.3	POM pictures of: a) a positive integer point defect, under crossed polarizers; b) same point defect as in a), between cross-polarizers with a 530nm retardation plate; c) same point defect as in a), between parallel polarizers, rotated anticlockwise. It should be noted that the four brushes also rotate counterclockwise, implying that this is a positive integer point defect; d) a Schlieren texture of a nematic liquid crystal, under crossed polarizers, showing positive and negative integer point defects. Schematic representation of some topological defects: e) negative semi-integer, $m = -(1/2)$; f) positive semi-integer, $m = +(1/2)$; g) negative integer, $m = -1$; h) positive integer, $m = +1$	4
3.1	Schematic representation of a simple twist. The nematic molecules are parallel to the z axis near the wall, and parallel to \vec{B} far from the wall. The applied magnetic field \vec{B} is parallel to the x axis. As the distance from the wall increases, the nematic molecules present an angle β , going from 0 near the wall, to $\pi/2$ far from the wall[8].	10
3.2	Symmetries of the system "cylinder + field": a) Planar axial anchoring, no field: $D_{\infty h}$, for simplicity only one mirror plane parallel to the cylinder axis and one twofold axis orthogonal to it are shown; b) Planar axial anchoring + field orthogonal to the cylinder: D_{2h} ; c) Planar axial anchoring + field oblique to the cylinder: C_{2v} ; d) Helical anchoring + field orthogonal to the cylinder: D_2	11
3.3	Fiber with axial anchoring in the magnetic field orthogonal to it: a) and b) are the two ground states.	12
3.4	Magnetic field of a cylindrical magnet acting as a trap for disclination loops.	12
3.5	The chirogyral effect: tilt of the captive disclination loops with respect to the axis of the fiber with a planar helicoidal anchoring inserted in a nematic homeotropic sample with the director field oriented in z direction.	14
3.6	Fiber of diameter $D = 28\mu m$, drawn by hand from an anisotropic 63% HPC-in-water solution, has been inserted in a homeotropic sample, treated with egg yolk, of thickness $d = 100\mu m$, through one of its two free edges. The sample was filled with the nematic liquid crystal EN18. a) one captive disclination loop (cdl); b-c) stretching of the initial disclination loop by electrohydrodynamic turbulence; d-h) relaxation of disclination loops created by turbulence; all loops but one collapse.	15

3.7	Generation of captive disclination loops by the electrohydrodynamic turbulence: a) one disclination loop captive on a HPC fiber inserted in a homeotropic cell of the nematic EN18; b) stretching of the initial captive disclination loop leads to formation of the strongly light scattering domain DSM2 containing a finite density of disclinations; c) growth of the DSM2 domain; d-g) elastic relaxation after switching the AC field off unveils the existence of six new pairs of disclination loops generated by the turbulent flow.	16
3.8	Principle of the experiment. Captive disclination loops threaded on a Nylon fiber, inserted into a sample with homeotropic anchoring, filled with nematic liquid crystal 5CB, are submitted to an oblique and inhomogeneous magnetic field created by cylindrical magnets: a) Photograph of setup; b) perspective view of the setup; c) closer view of the setup.	17
3.9	Determination of the relaxation time τ characteristic of the magnetic trap: a) one frame showing one position of the captive disclination loop around the fiber, and the magnet orthogonal to the fiber axis; b) reslice of the image sequence.	18
3.10	Variation of the shape of the disclination loop, with the increasing of the distance between the magnets and the fiber. The distance d is expressed in μm	18
3.11	a) Plot of the position of the captive disclination loop versus the time of the movie; b) Plot of the inverse of time constant versus the inverse of the distance between the disclination loop and the magnets; c) Plot of the time constant versus the distance between the disclination loop and the magnets, represented by the red crosses, and the tilt angle versus the distance between the disclination loop and the magnets, represented by the blue crosses.	19
3.12	Principle of the experiment. Captive disclination loop threaded on a Nylon fiber, inserted into sample with homeotropic anchoring, filled with nematic liquid crystal 5CB, are submitted to an horizontal homogeneous magnetic field, created by two cylindrical magnets: a) Photograph of the setup; b) perspective view.	20
3.13	Reslice of the image sequence, showing the increasing of the velocity of the disclination loop, with the increasing of the field angle between the disclination loop and the magnets.	21
3.14	a) Plot of the velocity of the disclination loop versus the field angle $\theta(\theta = \pi - \Phi)$ between the fiber main axis and the horizontal homogeneous magnetic field created by the two magnets. The plain line in this graph represents the best linear fit to experimental results in the interval $[-50^\circ, 50^\circ]$; b) symmetry relationship explaining the odd dependence of v on Φ	22
3.15	a) Photograph of the electrospinning setup: 1- infusion pump KDS100; 2- syringe; 3- coaxial shield ring; 4- target. The flow rate, the voltage used and the distance between the needle and the target were, respectively: $0.02 mlh^{-1}$, $20kV$ and $15cm$. b) Photograph of the target, where we can see the plastic frame, coated with double sided adhesive tape, glued on top of the aluminum stripes separated by $6mm$	23
3.16	Photograph of the setup: 1- magnet; 2- microscope lens; 3- sample; 4- microscope platinum; 5- magnet holder. Electrospinning fibers inserted in a sample with homeotropic anchoring, and filled with the nematic liquid crystal 5CB, are submitted to an horizontal and homogeneous magnetic field, created by two cylindrical magnets. The angle between the fibers main axis and the magnets is controlled by the angles marked in the platinum. The microscope used is a polarized light microscope.	24

-
- 3.17 POM pictures of cellulose acetate fibers, produced from a CA solution (12%w/w), in a homeotropic sample: a) under crossed polarizers; b) between cross-polarizers with a 530nm retardation plate. The different colors surrounding the fiber, yellow and blue, show us that there are different orientation of the director field \vec{n} along the fiber[27]. The average diameter of the fibers is $4\mu m$. These fibers induce disclination loops which can be seen easily in these two photographs, that are perpendicular to the fiber main axis, due to the planar anchoring on the fiber surface and the homeotropic anchoring of the sample walls. 24
- 3.18 Picture a captive disclination loop on a nylon fiber, where the equilibrium distance h , as well as R , f_L and f_r are schematically represented. The scale bar corresponds to $50\mu m$ 25
- 3.19 POM pictures of the natural fibers taken from the plant called *Ornithogalum thyrsoides*, in a homeotropic sample: a) under crossed polarizers; b) between cross-polarizers with a 530nm retardation plate; c) between parallel polarizers. We can easily see that these fibers also induce disclination loops. Through a close observation of the picture b), we noticed that the direction of the nematic molecules in the regions near the disclination loops varies. This could be seen by the change of colors between yellow and blue[27]. The average diameter of the fibers is $2\mu m$ 26

1.1 Aims of the present work

Liquid crystals (LCs) response to electric and magnetic fields enables their widespread technological applications. The uniaxial nematic phase is the most studied and is characterized by a long-range orientational order and the appearance of dark, flexible filaments known as disclination lines. The precise control of the presence and movement of these lines, corresponding to singularities in the molecular alignment, opens new horizons to LCs applications and to man-made soft materials.

It has been shown recently by Xiaoguang Wang et al.[1] that the cores of singular defects appearing optically as point defects are, in fact, nanometer-sized closed-loops. In addition, it was also shown by Xiaoguang Wang et al.[2] that these nanoscopic environments can trigger processes of molecular self-assembly in a very selective way.

In this work, micrometer-sized captive disclination loops will be manipulated by the application of magnetic fields. In particular, the behaviour of these loops, under the action of oblique and/or inhomogeneous magnetic fields, threaded on Nylon, natural and electrospun fibers immersed in homeotropic nematic cells will be addressed. More precisely, in the case of using nylon fibers two different setups will be built: the first one to study the behaviour of the captive disclination loops when submitted to an oblique and inhomogeneous magnetic field created by cylindrical magnets. The trajectory of the disclination loop as function of time, and also the time constant and the tilt angle of the loop, when the distance between the fiber and the magnets is changed, will be calculated; the second setup will allow to study the behaviour of these loops when an horizontal and homogeneous magnetic field, created by two cylindrical magnets is applied, and also the influence on the velocity of the disclination loop when the angle θ between the fiber main axis and the cylindrical magnets is changed.

When using electrospun and natural fibers, horizontal and homogeneous magnetic field will be applied, with the aim to determine the behaviour of the captive disclination loops while using fibers with 1-2 μm diameter, much smaller than the Nylon fiber diameter ($\sim 60\mu m$). Lastly, we will try to determine the critical diameter from which the disclination loop doesn't vanish throughout the medium.

1.2 Liquid Crystals: Nematic Phase

A fourth state of matter - liquid crystals (LCs) - was discovered in the late nineteenth century, and it is described crudely as an intermediate state between the crystalline (solid) and the isotropic (liquid) state, sharing properties from the first one, such as optical properties, but also flows and adapts

the shape of the container, characteristics from the second one[3]. Liquid crystals, or mesomorphic materials can be classified in three main groups, based on their structures: nematics, columnar and smectics[4, 5].

Regarding the nematic phase, represented in Figure 1.1 a), which is the most studied among liquid crystalline phases, the anisotropic molecules exhibit long-range orientational order, and no positional order[3, 4], defined by the director \vec{n} , schematically represented in Figure 1.1 b)[5, 6, 7]. The deviation between an arbitrary molecule and the director \vec{n} is given by θ , schematically shown in Figure 1.1 b). The fact that not all molecules point in the same direction is due to the existence of thermal fluctuations. The orientational order is expressed by the order parameter[4], given by 1.1[8]:

$$\langle S \rangle = \frac{1}{2} \langle 3 \cos^2(\theta) - 1 \rangle \quad (1.1)$$

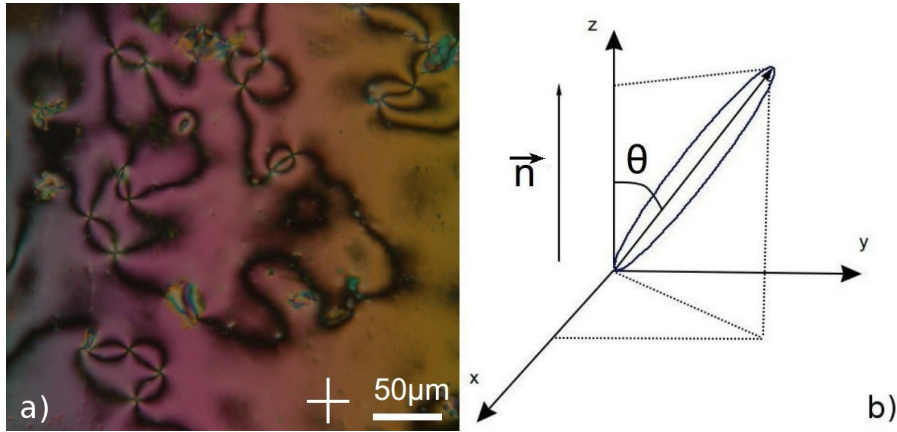


Figure 1.1: a) POM picture of the nematic phase, between cross-polarizers; b) Schematic representation of the director \vec{n} , showing the average orientation of the calamitic molecules, and θ , the deviation between an arbitrary nematic calamitic molecule and the director \vec{n} .

The order parameter is a thermodynamic parameter that decreases with increasing temperature, due to the fact that in the isotropic phase the molecules are randomly distributed, $S = 0$. For an ideal crystal, the order parameter is equal to 1[6, 7, 9].

Nematics (from Greek “ $\nu\eta\mu\alpha$ ” - thread) owes its name to disclination defects, which appeared as threads. These threads have been called "disclination lines" by Frank, and can be easily seen when a nematic phase is observed under polarized light. We will discuss this in more detail along section 1.2.3[4, 6, 10].

1.2.1 Frank's continuous elastic theory

We can assume that nematic liquid crystal molecules have a long distance orientational order as explained in section 1.2. However, the nematic phase can experience orientational deformations. These deformations of the director field, which increases the free energy of the system are splay, twist and bend, and are schematically represented in Figure 1.2. The Frank free energy expression can be simplified and given by the equation 1.2[3, 4, 5, 7, 11, 12, 13, 14], considering also the

influence of a magnetic field:

$$F_d = \frac{1}{2}K_{11}(\text{div } \mathbf{n})^2 + \frac{1}{2}K_{22}(\mathbf{n} \cdot \text{rot } \mathbf{n})^2 + \frac{1}{2}K_{33}(\mathbf{n} \times \text{rot } \mathbf{n})^2 - \frac{1}{2}\varepsilon_0\varepsilon_a(\mathbf{n} \cdot \mathbf{B})^2 \quad (1.2)$$

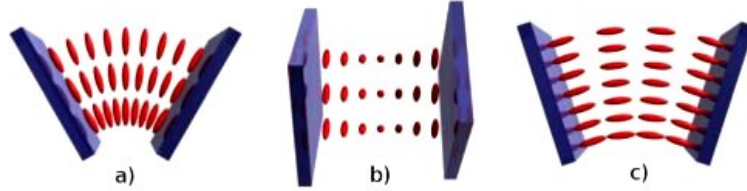


Figure 1.2: Schematic representation of the different types of elastic deformations in nematic liquid crystal: a) Splay (K_{11}); b) Twist (K_{22}); c) Bend (K_{33})[9].

Where $-\frac{1}{2}\varepsilon_0\varepsilon_a(\mathbf{n} \cdot \mathbf{B})^2$ is the magnetic field component. Regarding this equation, the constants K_{11} , K_{22} and K_{33} are called Frank elastic constants, and refers to the ability of the director to prevent Splay, Twist and Bend deformations, respectively. These constants are dependent on the nematic temperature, being generally positive, to ensure the stability of the system[6, 7].

1.2.2 Surface Anchoring

Assuming that the Liquid Crystal (LC) is confined between two substrates, which can be subjected to different treatments, the LC's director can be easily manipulated, depending on the different anchoring conditions of the sample substrates. Several types of molecular orientation can be promoted, where we can distinguish the following two: planar and homeotropic alignment. The first one can be achieved by rubbing the surfaces unidirectionally, which means that the director \mathbf{n} of the nematic liquid crystal stays parallel to the surface, Figure 1.2 a) and b). Regarding the homeotropic anchoring that is more difficult to achieve than the previous one, due to the fact that most surfaces, including glass, provide planar alignment. In this configuration, the director \mathbf{n} is perpendicular to the surfaces, Figure 1.2 c). To induce this anchoring, usually the substrates are treated with lecithin[13, 15, 16].

1.2.3 Topological Defects

Defects in liquid crystals can be described as specific regions, within the sample, where the orientation of the molecules is ill-defined. They may be caused by a continuous symmetry breaking, when a phase transition occurs, or due to an application of an external field. The existence of these singularities can increase the free energy of the system[7, 17].

Previous studies indicate that defects in LCs can be classified based on their dimension: point defects, 0-dimensional structure, when the defect is at a point; line defects, or disclination lines, a 1-dimensional structure; and defect walls, a 2-dimensional structure[7, 18]. The topology and the location of these defects, as well as their distributions, may change with temperature, and also with the nematic anchoring conditions[15, 16].

When analysing a nematic sample between crossed polarizers, it's very common to find a texture called Schlieren texture[19], Figure 1.1 a) and Figure 1.3 d), wherein point defects emanating black brushes, where the orientation of the molecules is parallel or perpendicular to the polarizes[3]. These

spots are both point defects, and can have two or four brushes[20]. In the first case, these point defects correspond to thin threads, and are associated with the end of singular stable disclinations. These defects are associated with the topological charge $m = \pm(1/2)$ [21], due to a rotation of the molecules main axis by $\pm\pi$ around the defect. The topological charge is given by the number of brushes divided by 4. The positive sign is assigned to clockwise[3]. When there are four brushes, Figure 1.3 a), the topological charge associated is $m = \pm 1$, due to a rotation of the director by $\pm 2\pi$ around the point[3, 20, 21], corresponding to point defects that are isolated.

Point defects are subdivided in boojums and hedgehogs. The first one is a surface point defect, owing to the fact that they can only exist on the boundaries of the medium, and cannot move inside the bulk. On the other side, hedgehogs are called bulk point defects, due to the fact that they can exist either on the surface but also in the volume[10, 18, 20, 21]. They can also also exhibit radial or hyperbolic configuration[17].

Given the equation 1.2, we can use the one-constant approximation: $K_{11} = K_{22} = K_{33} = K$, and assuming that a disclination line is located in tin the xy plane, the director field is given by: $\mathbf{n}(r) = [\cos \theta(x, y), \sin \theta(x, y), 0]$ [22]. Therefore, this gives rise to the equation: $f_d(\mathbf{r}) = \frac{1}{2}K(\theta_x^2 + \theta_y^2)$ [22]. Due to the fact that the system tends to minimize the free energy, we obtain: $\nabla_{xy}^2 \theta = 0$ [3]. Using polar coordinates, and due to the relation between θ and ϕ , the equation that describes the director's configuration around disclinations is given by 1.3[3]:

$$\theta(\phi) = m\phi + \theta_0 \quad (1.3)$$

Where $\phi = \arctan(y/x)$, θ_0 is a constant and m is a positive or negative integer or semi-integer. Some possible configurations of \vec{n} are schematically represented in Figure 1.3 e-h)[7].

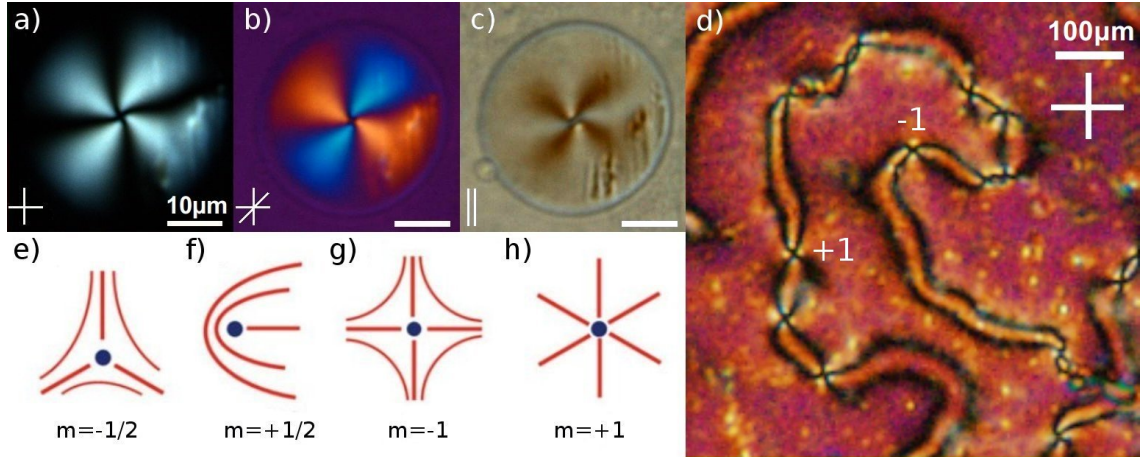


Figure 1.3: POM pictures of: a) a positive integer point defect, under crossed polarizers; b) same point defect as in a), between cross-polarizers with a 530nm retardation plate; c) same point defect as in a), between parallel polarizers, rotated anticlockwise. It should be noted that the four brushes also rotate counterclockwise, implying that this is a positive integer point defect; d) a Schlieren texture of a nematic liquid crystal, under crossed polarizers, showing positive and negative integer point defects. Schematic representation of some topological defects: e) negative semi-integer, $m = -(1/2)$; f) positive semi-integer, $m = +(1/2)$; g) negative integer, $m = -1$; h) positive integer, $m = +1$.

1.2.4 Captive disclination loops on fibers

We have already introduced and discuss the existence of point defects and disclination lines, but regarding the first ones, more precisely hedgehogs ($m = \pm 1$), they can be transformed into disclination loops with $m = \pm(1/2)$, first notice by Lavrentovich and Terentijev[23], when a transition between radial and hyperbolic hedgehogs occurs[24, 25].

It has been generally admitted that due to their tension disclination loops in nematic liquid crystal inevitably collapse. It has been show recently by M.H. Godinho et al.[26] that this is not the case when disclination loops are threaded on fibers. In particular such captive disclination loops exist in nematic droplets suspended in cellulosic fibers. Later, the behaviour of these loops was studied using hydroxypropylcellulose(HPC) and Nylon fibers, both with planar anchoring, in homeotropic cells containing nematic liquid crystal[27]. In the case of using HPC, or even twisted nylon, the planar anchoring of the nematic becomes helicoidal near the fiber, resulting then, in an effect called Chirogyral Effect, wherein the disclination loop is tilted, instead of being perpendicular to the fiber[27].

1.2.5 External Fields

It is known that nematics are sensitive to external fields, due to the fact that the local orientation of the molecules and the thermal fluctuations of the director can be changed by the application of magnetic or electric fields, leading to changes in the bulk sample[28]. When a magnetic field is applied, the nematic sample tends to be parallel to the field when its diamagnetic anisotropy is positive ($\Delta_\chi > 0$), and perpendicular when is negative ($\Delta_\chi < 0$)[3, 11]. When a magnetic field (\mathbf{B}) is applied, the acquired magnetization by each molecule (\mathbf{m}) is given by 1.4[4]:

$$\mathbf{m} = \frac{1}{\mu_0} [\chi_\perp \mathbf{B} + \Delta_\chi (\mathbf{B} \cdot \mathbf{n}) \mathbf{n}] \quad (1.4)$$

Where μ_0 is the permittivity in free space.

Regarding the topological defects, apart from the fact that they can be created when a phase transition occurs, they can be also formed when these fields are applied[3, 7].

Experimental and Characterization Techniques

Liquid crystal used during the experiments was the nematic liquid crystal 4'-n-pentyl cyanobiphenyl (5CB), exhibiting a nematic phase between 18° C and 34° C, and also the nematic liquid crystal EN18.

In the first setup, the cell containing the nematic liquid crystal was made of two overlapping glass plates with 10mm width, 20mm length and 1mm of thickness. One plate was fixed while the second one, supported by a simple mechanical system, was mobile. More precisely, the distance h between the two plates as well as their parallelism can be controlled. The inner surfaces of the two glass plates were treated with egg yolk with the aim to induce a homeotropic anchoring of the nematic liquid crystal. The cell was filled with the nematic liquid crystal 5CB.

The Nylon fiber (fishing line 0.2mm in diameter) was stretched between the collinear axes of two stepping motors controlled independently. By this means the fiber can be twisted precisely. The nematic cell, fixed on a xyz translation stage, was moved towards the fiber and by this means the Nylon fiber was introduced into the sample.

After this operation, usually one or more captive disclination loops were formed on the fiber. Otherwise, we had to create a turbulent flow in the sample, by a vigorous motion of the fiber. Such a turbulent flow stretches disclination lines and results in generation of new captive loops. This is going to be explained in more detail in section 3.5. The sample was observed in transmission mode with an optical system made of a microscope objective and a CCD camera.

As shown in Figure 3.8 b), the inhomogeneous magnetic field \vec{B} was created by a long cylindrical magnet, almost parallel to the z axis. The magnet was supported by a xyz translation stage, allowing to control its position with respect to the fiber and to the disclination loop. We have made a series of experiments in which the z position of the magnet was kept constant and only the x and y positions were modified.

When the captive disclination loop is located in the point O (see Figure 3.4) where the field \vec{B} is orthogonal to the fiber, it does not move. But if it is located in positions 1 or 1', where the magnetic field is oblique with respect to the fiber, the disclination loop will move in the $-x$ or x direction, respectively.

During experiments, the magnet was first positioned in a way that the loop was located outside of its equilibrium position O. Then, the motion of the captive disclination loop was recorded as a sequence of images, usually taken at the rate of one image every twenty seconds. Subsequently, the sequence of images was treated using the softwares ImageJ and IgorPro, with the aim to determine the characteristic relaxation time of the return of the loop into the equilibrium position O. More details about this treatment will be given in section 3.

In the experiment illustrated by the series of eight pictures in Figure 3.6, section 3.5, a fiber of diameter $D = 28\mu m$, drawn by hand from an anisotropic 63% HPC-in-water solution, has been inserted in a homeotropic sample, also treated with egg yolk, of thickness $d = 100\mu m$, through one of its two free edges. The sample was filled with the nematic liquid crystal EN18.

In the second setup, as shown in Figure 3.12 a) and b), the liquid crystal cell was assembled from two glass plates separated by a plastic spacer of thickness $0.6mm$. The cell was then fixed with an epoxy glue on the top of a cylindrical support conceived specially for the purpose of the experiment with horizontal magnetic fields. The plans of this support were drawn with the software SolidWorks, and printed using a 3D printer. In order to enable the application of an horizontal and homogeneous magnetic field, a second part - the magnet holder - was build by the same method. It had a shape of a ring equipped with radial cylindrical holes in which magnets were inserted. The inner diameter of the ring was identical with the outer diameter of the first part, so that magnets can be rotated around the z axis, see Figure 3.12 a). Like in the previous experiment, the Nylon fiber was stretched between the axes of stepping motors, and introduced into the sample, as shown in Figure 3.12 a).

The motion of the captive disclination loop driven by the horizontal and homogeneous magnetic field was recorded, and analyzed in the same way as in the previous experiment.

The electrospinning fibers were prepared from cellulose acetate (CA), obtained from 12% CA ($M_n = 50000gmol^{-1}$), in a homogeneous mixture of 66.6% (w/w) acetone and 33.3% (w/w) DMac. The viscous solution was poured into a $2ml$ syringe with $4.5mm$ diameter fitted with a 27-gauge needle, with $0.2ml$ inner diameter. The syringe was then placed on a infusion pump (KDS100), to control the flow. The conducting ring with 15 cm in diameter was held coaxially with the needle tip, and electrically connected to it. Then they were both connected with a positive output of a high voltage supply (Glassman EL 30kV). After applying the electric potential, the highly viscous CA solution was fed to the syringe-tip as a constant flow rate of $0.02mlh^{-1}$. The voltage used was 20kV, and the distance between the nozzle and the collector was 15cm. The setup is illustrated in Figure 3.15 a). The fiber collectors was made of a plastic frame ($6 \times 22mm$), coated with double sided adhesive tape, glued on top of two aluminum stripes distanced $0.6cm$ from each other, see Figure 3.15 b). During the process the humidity was around 50% at room temperature, $24^\circ C$.

The samples were made of two overlapping glass plates ($10mm \times 20mm^2$), $1mm$ of thickness, threated with lecithin as well, and the plastic support containing the suspended fibers was placed in the middle. An epoxy glue was used to seal the sample. The samples were then filled with nematic 5CB.

The natural fibers used in the experiments were taken from the plant called *Ornithogalum thyrsoides*[29], and they were suspended in the same plastic support. The samples were prepared using the same method. The samples were observed using a transmission mode microscope, equipped with polarizers, a 530 nm retardation plate, a heating/cooling stage and a camera. The image sequences recorded were analyzed with the software VLC media player.

3.1 Planar Axial Anchoring

Let us consider first a cylinder with planar axial anchoring $\vec{a} // \vec{x}$ (see Figure 3.2), immersed in a nematic. In the absence of fields and other surface conditions the director field \vec{n} would take the direction parallel to the cylinder axis \vec{x} . The symmetry of this ground state is $D_{\infty h}$ (see Figure 3.2 a)).

When a magnetic field \vec{B} is applied in the direction \vec{z} orthogonal to the cylinder, the symmetry $D_{\infty h}$ is broken into D_{2h} (see Figure 3.2 b)) and the director field will be distorted: far from the cylinder it will take the direction of the field while on the cylinder surface it will remain parallel to \vec{x} .

As shown in Figure 3.3 two distorted ground states a) and b) are possible. Taken separately they are symmetrical only with respect to the longitudinal mirror plane xz and to the twofold axis $C_2 // \vec{y}$ orthogonal the field. All other symmetry operations of the group D_{2h} (mirror planes xy and yz and the two-fold axis $C_2 // \vec{B}$) exchange the two ground states.

The same symmetry breaking occurs when the cylinder immersed in a nematic is submitted to the action of glass plates with homeotropic anchoring[30].

In the two ground states generated by the magnetic field, the distortion is localized in a cylindrical shell whose thickness is given by the so-called magnetic coherence length ξ [8], which due to its importance must be explained in more detail, starting with the case of a simple twist. First, we have to take into account the effects of a magnetic field and a wall on the alignment of the nematic molecules, in the case where the wall is in the xoy plane, and the magnetic field \vec{B} is applied in parallel to the x axis, as shown in Figure 3.1. We can observe that near the wall the nematic molecules are parallel to the z axis, and far from the wall they are parallel to \vec{B} [8]. This means that there is a transition layer, near the wall, where the molecules are parallel to it, with the addition of presenting an angle $\beta(y)$ with the z direction, as represented in Figure 3.1. This can be classified as a distorted state, where the magnetic torque $\Gamma_{\mathbf{M}}$ acting on the magnetization \mathbf{M} is given by 3.1[8]:

$$\Gamma_{\mathbf{M}} = \chi_a (\mathbf{n} \cdot \mathbf{B}) \mathbf{n} \times \mathbf{B} \quad (3.1)$$

Taking that into account, in this case, $\Gamma_{\mathbf{M}}$ is parallel to the y axis, and considering a section ($1 \times 1 \text{ cm}$) in the xoy plane, from y to $y + dy$, the section experiences a surface and a bulk torque. Adding these torques, the equilibrium equation is given by 3.2:

$$K_2 \frac{d^2 \beta}{dy^2} + \chi_a B^2 \sin \beta \cos \beta = 0 \quad (3.2)$$

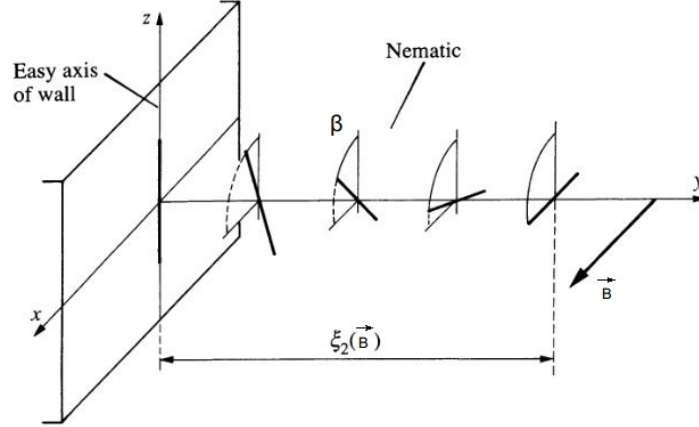


Figure 3.1: Schematic representation of a simple twist. The nematic molecules are parallel to the z axis near the wall, and parallel to \vec{B} far from the wall. The applied magnetic field \vec{B} is parallel to the x axis. As the distance from the wall increases, the nematic molecules present an angle β , going from 0 near the wall, to $\pi/2$ far from the wall[8].

Where $\xi_2(\vec{B})$ is a length defined by 3.3:

$$\xi_2(B) = (K_2\chi_a)^{1/2}/B \quad (3.3)$$

Substituting in the equation 3.2 and integrating, and due to the fact that far from the wall $\beta = \pi/2$, we come to the equation 3.4:

$$\xi_2 \frac{d\beta}{dy} = \pm \cos \beta \quad (3.4)$$

Where both solutions are possible. Choosing one of them, and resolving the equation by using a change of variable[8], the result is given by 3.5:

$$t = \exp(-y/\xi_2) \quad (3.5)$$

Where $t = \tan\left(\frac{(\pi/2)-\beta}{2}\right)$. This shows that $\xi_2(B)$ can be considered as the transition layer.

Regarding a different case, where the applied magnetic field \vec{B} is parallel to the y axis, it is not just a case of a simple twist, but a combination of splay and bend[8]. These distortions are associated with the elastic constants K_{11} and K_{33} , respectively, where their lengths (ξ_i) are similar. Thus, using the one-constant approximation already discussed in section 1.2.3 ($K_{11} = K_{22} = K_{33} = K$), the magnetic coherence length is given by 3.6[8]:

$$\xi(B) = \sqrt{\frac{\mu_0 K}{\chi_a}} \frac{1}{B} \quad (3.6)$$

and the elastic energy per unit surface of the distorted boundary layer is given by:

$$F = \frac{1}{2} \frac{K}{\xi} \quad (3.7)$$

3.2 Tilted magnetic field, translation of disclination loops

When the magnetic field is oblique to the cylinder (for example tilted in the direction of the x axis as shown in Figure 3.2 c)), the symmetry D_{2h} is broken to C_{2v} and the two ground states are

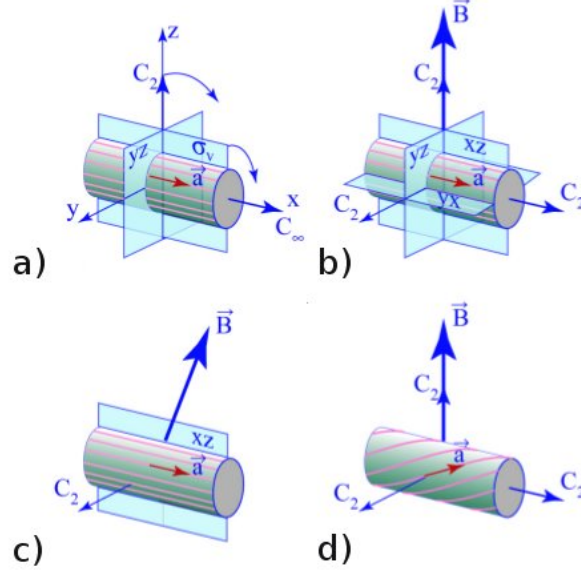


Figure 3.2: Symmetries of the system "cylinder + field": a) Planar axial anchoring, no field: $D_{\infty h}$, for simplicity only one mirror plane parallel to the cylinder axis and one twofold axis orthogonal to it are shown; b) Planar axial anchoring + field orthogonal to the cylinder: D_{2h} ; c) Planar axial anchoring + field oblique to the cylinder: C_{2v} ; d) Helical anchoring + field orthogonal to the cylinder: D_2 .

no more related by any symmetry operation. If the angle between the magnetic field and cylinder is written as:

$$\frac{\pi}{2} - \Phi = \frac{\pi}{2}(1 - \epsilon) \quad (3.8)$$

where $\epsilon \ll 1$, then the distortion energy of states **a** and **b** becomes:

$$F_{a/b} = (1 \pm \epsilon)^2 \frac{K}{2\xi} \quad (3.9)$$

When the two possible states **a** and **b** coexist on the fiber, there must be a disclination loop at the junction between them. This can be easily checked by following the director orientation on the circuit 12341 drawn with dashed line in Figure 3.3. At the starting point 1 the director is (0,0,1) while after the whole turn of the circuit it becomes (0,0,-1).

The energies per unit surface of the boundary layers adjacent to the disclination loop F_a and F_b can be seen as forces per unit length pulling on the loop, respectively, in $-\vec{x}$ and \vec{x} directions. The resultant force

$$f = F_b - F_a = -\frac{2K}{\xi} \frac{2}{\pi} \Phi \quad (3.10)$$

will pull the loop in the \vec{x} direction when the tilt angle of the magnetic field $\vec{\Phi}$ is positive. As a result, the disclination loop will move in the \vec{x} direction, as observed in experiments.

When other disclination loops coexist on the fiber then their sequence can be represented as:

$$\mathbf{a} - DL_1 - \mathbf{b} - DL_2 - \mathbf{a} - DL_3 - \mathbf{b} \dots \quad (3.11)$$

In this sequence, the ground states **a** and **b** are located respectively on left and right sides of loops DL_1 and DL_3 . In the case of the loop DL_2 the positions of the ground states are inverted so that the force f given by equation 3.10 changes its sign.

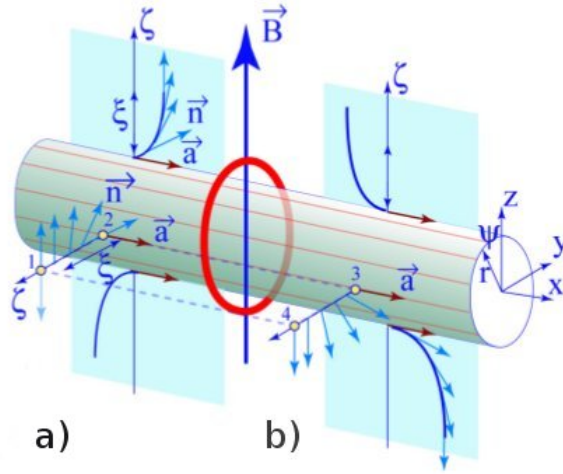


Figure 3.3: Fiber with axial anchoring in the magnetic field orthogonal to it: a) and b) are the two ground states.

3.3 Trap-like action of an inhomogeneous magnetic field

Knowing that the magnetic field oblique with respect to the fiber generates the force f proportional to the field angle Φ (see equations 3.8 and 3.10) we are prepared to analyse the action of inhomogeneous magnetic fields such as the one of the cylindrical magnet used in our experiments.

As shown in Figure 3.4, the magnetic field of a cylindrical magnet has the axial symmetry with respect to the magnet axis \vec{z} .

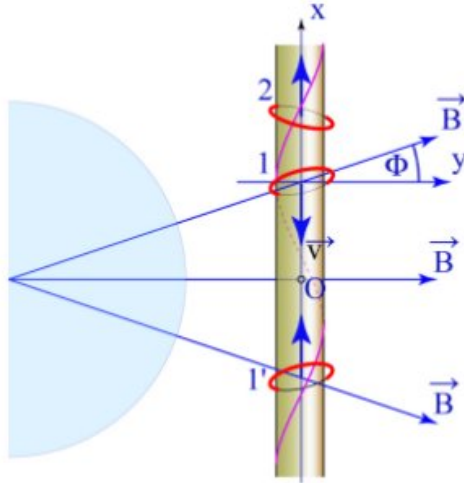


Figure 3.4: Magnetic field of a cylindrical magnet acting as a trap for disclination loops.

In this geometry, the angle Φ between the field and the axis y normal to the fiber varies as a function of the position x of the loop. In the first approximation, we can write:

$$\Phi \approx Ax \quad (3.12)$$

Then, using the equations 3.8 and 3.10 we obtain:

$$f = -Bx \quad (3.13)$$

with

$$B = \frac{2K}{\xi} \frac{2}{\pi} \quad (3.14)$$

Upon the action of the force f the dislocation loop will move with the velocity v given by:

$$B = v = \frac{dx}{dt} = \mu f \quad (3.15)$$

where μ is the mobility.

Finally using equation 3.13 and 3.15 we obtain the equation of motion:

$$\frac{dx}{dt} = -\mu Bx \quad (3.16)$$

Its solution:

$$x(t) = x_0 e^{-t/\tau} \quad (3.17)$$

3.4 Captive disclination loops, the chirogyral effect

As already introduced in section 1.2.4, the first observations of captive disclination loops were made in experiments with nematic[31] and cholesteric droplets[26] threaded on HPC fibers with planar anchoring. When the anchoring at the nematic (cholesteric)/air is homeotropic, each droplet must contain, for topological reasons, a defect with the topological charge $m = 1$: a disclination loop equivalent to a radial hedgehog.

Captive disclination loops were also observed on glass fibers with homeotropic anchoring immersed in planar nematic samples[32, 33]. In this geometry, disclination loops were generated in a controlled manner by the KibbleZurek mechanism during quenching from the isotropic into the nematic phase.

Recently, captive disclination loops were created and studied using HPC and Nylon fibers with a planar anchoring immersed in homeotropic nematic samples[27]. In the case when the planar anchoring on the fiber surface was helicoidal, due to the chirality of the polymer (HPC) or to the mechanical torsion of the fiber, the so-called chirogyral effect was observed (see Figure 3.5): the captive disclination loops are tilted with respect to the fiber axis by the angle η which is proportional in the first approximation to the helix angle α :

$$\eta = C_g(D/d)\alpha \quad (3.18)$$

The chirogyral coefficient $C_g(D/d)$ occurring in this formula, is a function of the ratio D/d between the fiber diameter D and the sample thickness d . In these first experiments, for symmetry reasons, disclination loops were rotating around the axis z parallel to the homeotropic anchoring on the sample surfaces.

Let us stress that the chirogyral effect was discovered previously in experiments with nematic droplets threaded on helicoidally-shaped fibers obtained by electrospinning where disclination loops were tilted with respect to the average axis of fibers[34].

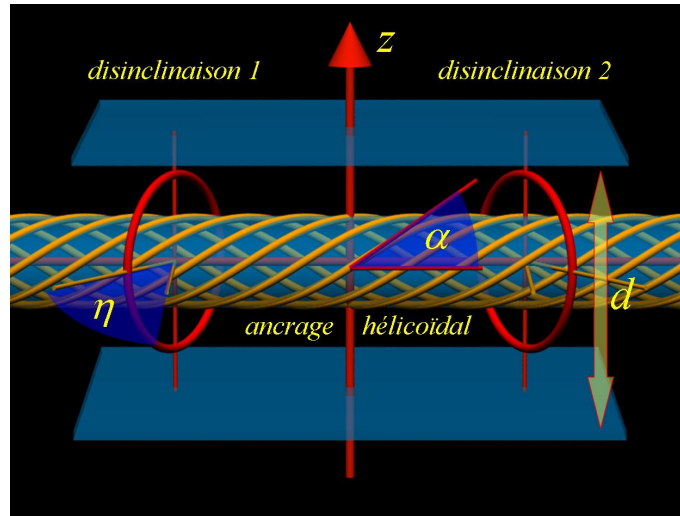


Figure 3.5: The chirogyral effect: tilt of the captive disclination loops with respect to the axis of the fiber with a planar helicoidal anchoring inserted in a nematic homotropic sample with the director field oriented in z direction.

3.5 Generation of captive disclination loops by electrohydrodynamic turbulence

In the experiment illustrated by the series of eight pictures in Figure 3.6, and already introduced in section 2, the sample contained, initially, one disclination loop threaded on the fiber. Subsequently, we applied a 100Hz , 50V , AC voltage to this EN18 sample with the negative dielectric anisotropy drove the electrohydrodynamic turbulence which stretched progressively the initial disclination loop and created the strongly light scattering area labelled DSM2 whose size is growing with time[35] as shown in Figures 3.6 b) and c). After switching the excitation off, due to the elastic relaxation, the density of disclination (length/unit volume) is rapidly falling down and a tangle of individual disclination can be distinguished in Figure 3.6 d). In Figure 3.6 f) only three loops are left. Their evolution in Figures 3.6 g) and h) shows that the one labeled *cdl* is captive and while the other two, *fdl1* and *fdl2*, are free and can collapse.

The outcome of this experiment is that the topology is a quite robust feature of the director field. Nevertheless, when a vigorous hydrodynamic turbulence is applied for a longer period, new captive disclinations can be created. This is shown in the series of seven pictures in Figure 3.7, where the number of captive disclinations increases from 1 (Figure 3.7 b)) to 13 (Figure 3.7 h)) by generation of six pairs of captive disclinations. We can also say that disclination loops can be created not only by the application of an electric field, like in the previous experiment, but also with the application of any other external field. In the following experiments, we are going to use two different approaches: a mechanical external field, where we create a turbulent flow in the sample, by a vigorous motion of the fiber; and a second one, an external magnetic field, created by cylindrical magnets.

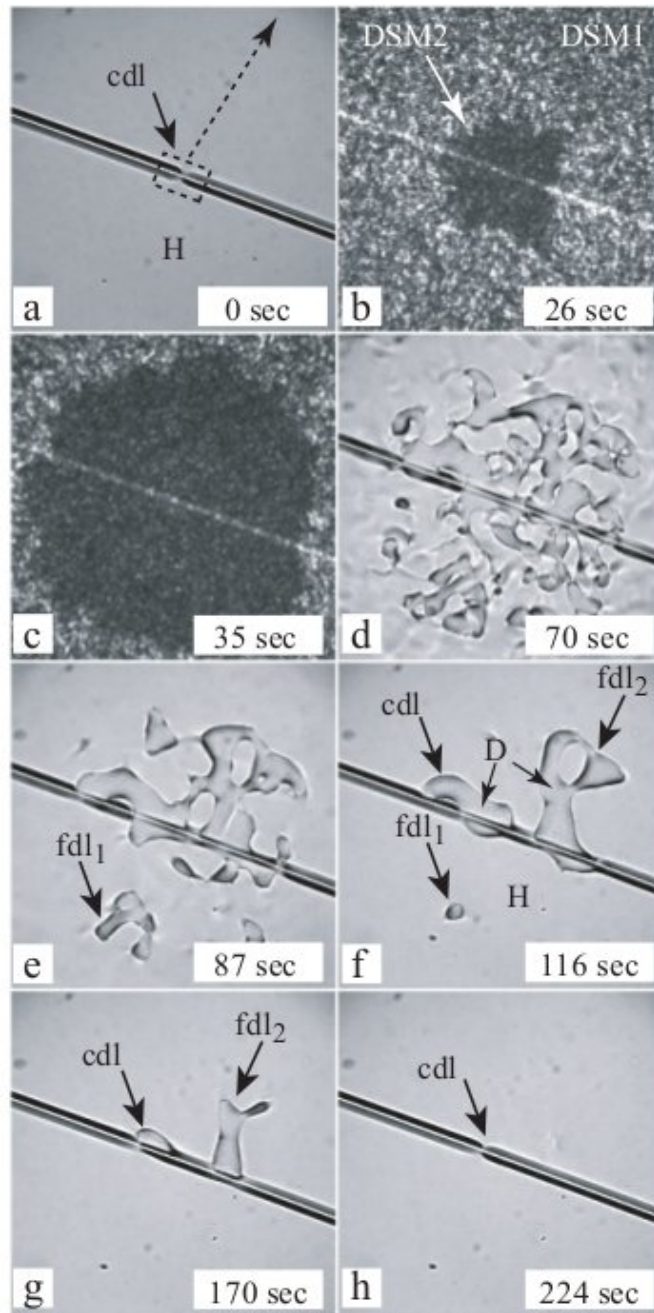


Figure 3.6: Fiber of diameter $D = 28\mu\text{m}$, drawn by hand from an anisotropic 63% HPC-in-water solution, has been inserted in a homeotropic sample, treated with egg yolk, of thickness $d = 100\mu\text{m}$, through one of its two free edges. The sample was filled with the nematic liquid crystal EN18. a) one captive disclination loop (cdl); b-c) stretching of the initial disclination loop by electrohydrodynamic turbulence; d-h) relaxation of disclination loops created by turbulence; all loops but one collapse.

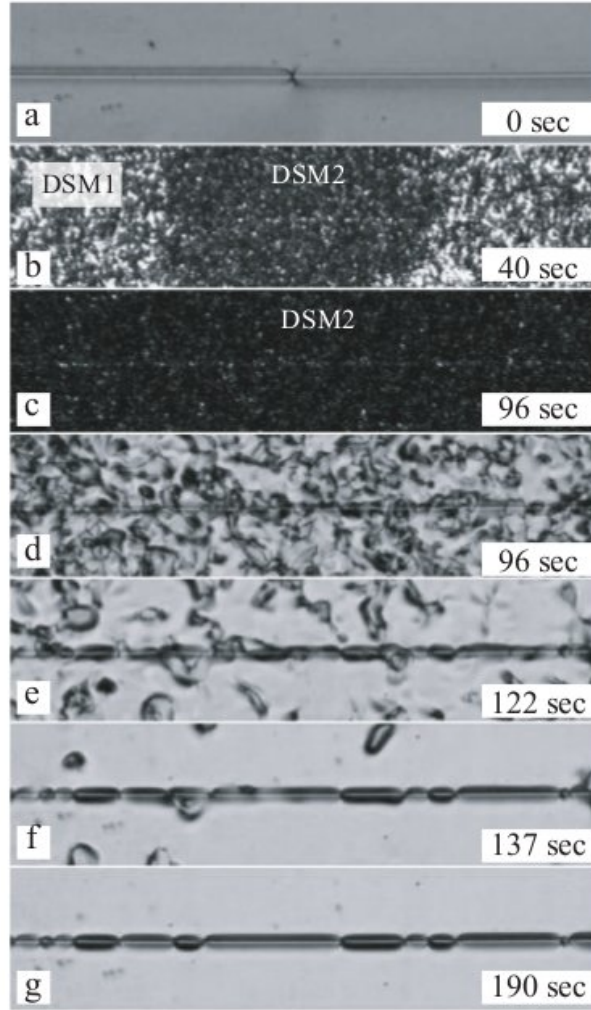


Figure 3.7: Generation of captive disclination loops by the electrohydrodynamic turbulence: a) one disclination loop captive on a HPC fiber inserted in a homeotropic cell of the nematic EN18; b) stretching of the initial captive disclination loop leads to formation of the strongly light scattering domain DSM2 containing a finite density of disclinations; c) growth of the DSM2 domain; d-g) elastic relaxation after switching the AC field off unveils the existence of six new pairs of disclination loops generated by the turbulent flow.

3.6 Magnetic Traps

With the purpose of studying the behavior of the captive disclinations loops threaded on nylon fibers, inserted in a sample with homeotropic anchoring, when an oblique and inhomogeneous magnetic field \vec{B} is applied, we build a setup, illustrated in Figure 3.8, and already explained in the beginning of section 2.

Before beginning the experience, the magnets were placed so that the disclination loop was not in its equilibrium position O . These positions may be 1 and $1'$, schematically represented in Figure 3.4. Then, in case the disclination loop is positioned in 1, the magnets were placed near the position $1'$, presenting an angle Φ between the field and the y axis normal to the fiber. This means that the disclination loop will be attracted to the magnet, due to the fact that the magnetic field

is now oblique with respect to the fiber, and will move in the $-\vec{x}$ direction, toward the position O , with a velocity v . The same will happen if the disclination loop is positioned in the $1'$ position, and the magnets near the position 1, resulting in the movement of the disclination loop in the \vec{x} direction, toward the position O . In this case, the position of the magnets was only changed in the \vec{x} direction. For each position of the magnets, a sequence of images was recorded, usually with a rate of one image every twenty seconds. The positions of the captive disclination loop versus the time of the movies are plotted in Figure 3.11 a). After that, we moved the magnets in the \vec{x} direction, but also in the $-\vec{y}$ direction, increasing the distance d between the magnets and the fiber. A sequence of images was recorded in the same way, for increasing distances.

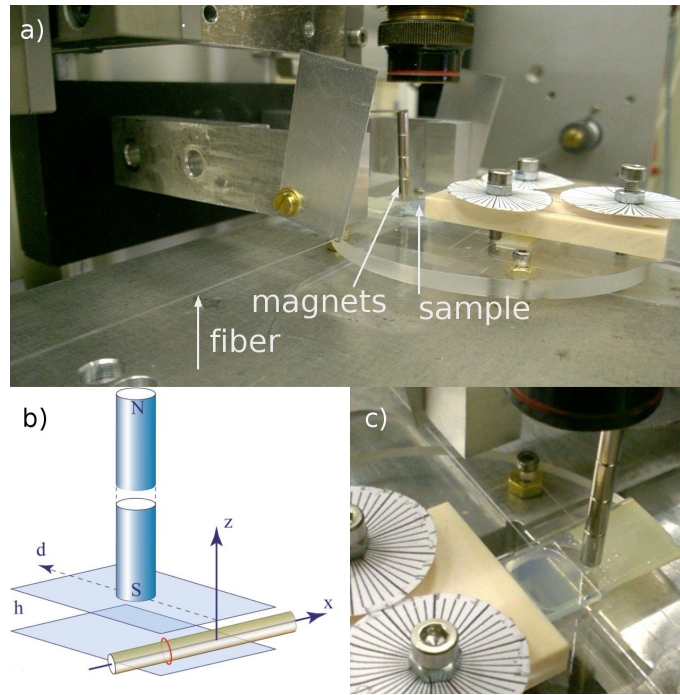


Figure 3.8: Principle of the experiment. Captive disclination loops threaded on a Nylon fiber, inserted into a sample with homeotropic anchoring, filled with nematic liquid crystal 5CB, are submitted to an oblique and inhomogeneous magnetic field created by cylindrical magnets: a) Photograph of setup; b) perspective view of the setup; c) closer view of the setup.

The image sequences recorded were analyzed using the software ImageJ. They were converted to grayscale, and imported as stacks. A typical image from one stack is shown in Figure 3.9 a). The segment AB visible here is parallel to the fiber, and crosses the disclination loop. Using the “reslice” command this segment was extracted from each image of the stack and the set of all segments was assembled into the image shown in Figure 3.9 b). Let us note that the segment AB is rotated by 90 degrees with respect to the Figure 3.9 a). It is obvious that the reslice image represents the trajectory $x(t)$ of the loop as a function of time. At the first sight, the shape of this trajectory seems to be exponential.

With the aim to extract the time constant τ , the positions (x, t) of the loop were measured using the multi-point selection option, and saved as an excel file. This data were then loaded into the IgorPro software as so called waves, and plotted as shown in Figure 3.11 a). Using the “analysis - fit” option the experimental points were then fitted to the exponential formula 3.19 using as

adjustable parameters coefficients x_0 and τ .

$$x(t) = x_0 e^{-t/\tau} \quad (3.19)$$

The inverse of the relaxation time $1/\tau$ was then plotted in Figure 3.11 b) as a function of the inverse of the distance d between the magnet and the fiber. Let us emphasize that both axes of the plot in Figure 3.11 b) are logarithmic. The reason for such a choice is that the expected dependence between $1/\tau$ and $1/d$ is approximatively given by the power law 3.20:

$$\frac{1}{\tau} = a \left(\frac{1}{d} \right)^\alpha \quad (3.20)$$

In such a log-log plot the exponent α corresponds to the slope of a straight line fitting the experimental points. The time constant τ and the tilt angle η versus the distance between the disclination loop and the magnets are represented in Figure 3.11 c). The shape of the disclination loop with the increasing of the distance between the magnet and the fiber is represented in Figure 3.10.

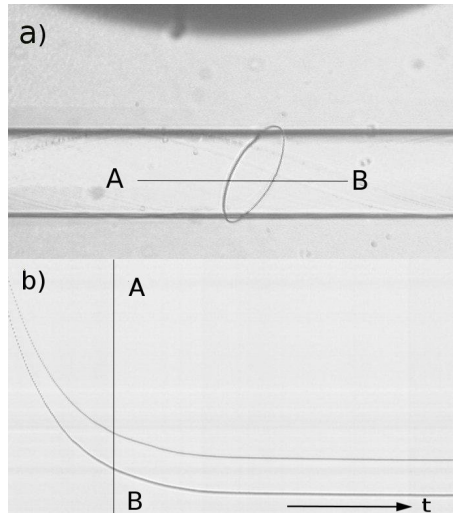


Figure 3.9: Determination of the relaxation time τ characteristic of the magnetic trap: a) one frame showing one position of the captive disclination loop around the fiber, and the magnet orthogonal to the fiber axis; b) reslice of the image sequence.

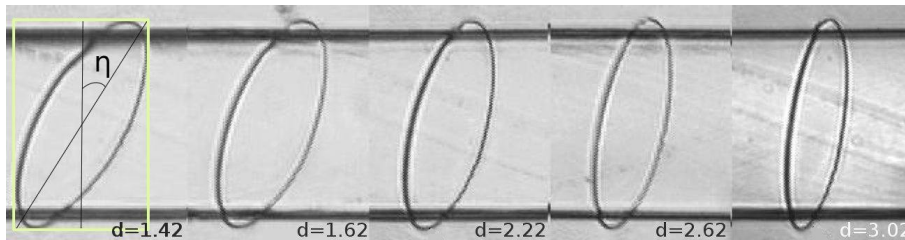


Figure 3.10: Variation of the shape of the disclination loop, with the increasing of the distance between the magnets and the fiber. The distance d is expressed in μm .

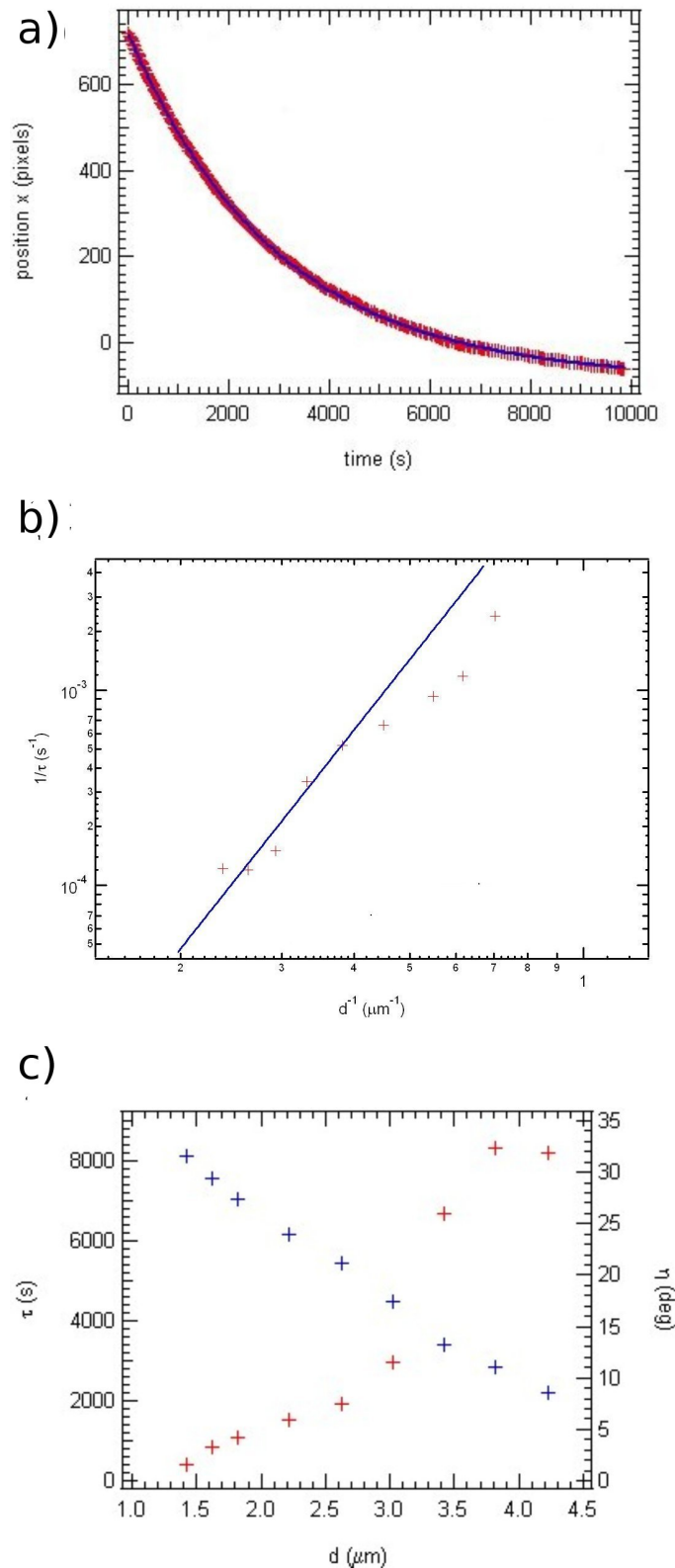


Figure 3.11: a) Plot of the position of the captive disclination loop versus the time of the movie; b) Plot of the inverse of time constant versus the inverse of the distance between the disclination loop and the magnets; c) Plot of the time constant versus the distance between the disclination loop and the magnets, represented by the red crosses, and the tilt angle versus the distance between the disclination loop and the magnets, represented by the blue crosses.

The Figure 3.11 b) shows clearly that the increasing of the distance between the disclination loop and the magnets translates into a increasing of the time constant. There is also a decreasing of the tilt angle of the disclination loops with the increasing of d , represented in Figure 3.11 c) and Figure 3.10.

These results are in agreement with the theoretical analysis in sections 3.1, 3.2 and 3.3.

3.7 Field induced translation of disclination loops

In this section, we studied the behavior of the captive disclination loops threaded on nylon fibers, inserted in a sample with homeotropic anchoring, when subjected to an horizontal and homogeneous magnetic field \vec{B} , created by two cylindrical magnets. For this purpose, a second setup was build, already described in section 2, and illustrated in Figure 3.12.

After inserting the nylon fiber into the sample, the magnets were initially placed in the magnet holder with an angle $\theta = 0$, wherein $\theta = \pi - \Phi$. This means that, in the beginning of the experience, the magnets were parallel to the fiber main axis (see Figure 3.12 b)). The angle θ ranged from 0 to 2π , every 5 degrees, around the z axis, clockwise, with the help of a circumference made of paper with lines drawn every 5 degrees. We recorded sequences of images of a loop moving upon the action of an horizontal and homogeneous magnetic field for each angle θ .

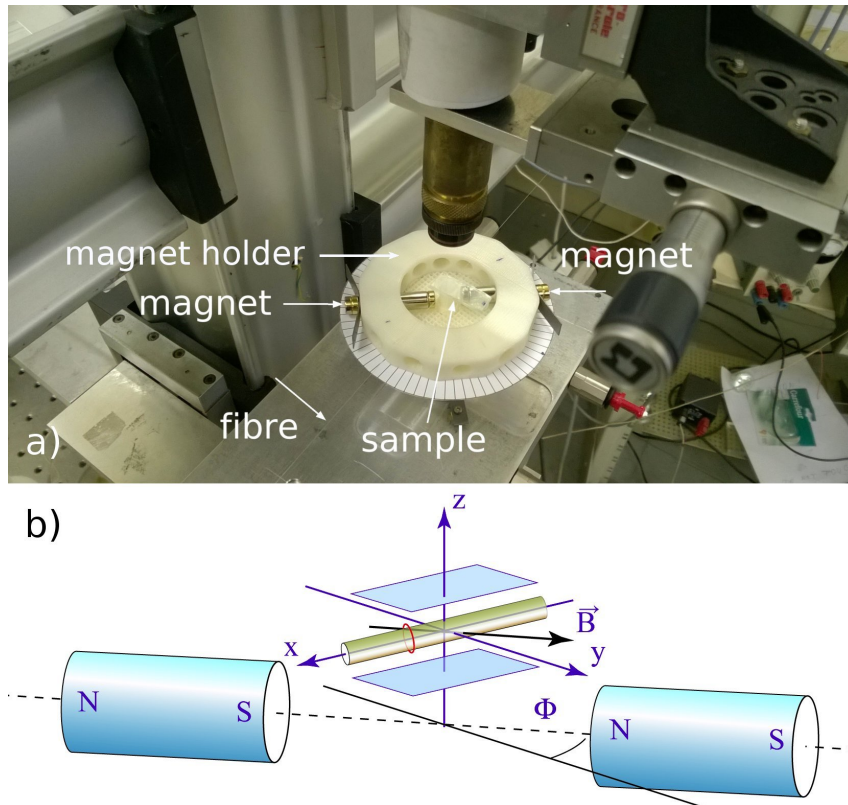


Figure 3.12: Principle of the experiment. Captive disclination loop threaded on a Nylon fiber, inserted into sample with homeotropic anchoring, filled with nematic liquid crystal 5CB, are submitted to an horizontal homogeneous magnetic field, created by two cylindrical magnets: a) Photograph of the setup; b) perspective view.

The analysis of the image sequences was then identical to what was done in section 3.5. For example, on the spatio-temporal cross section obtained by the reslice command (see Figure 3.13) the velocity of the disclination loop is given by the slope of the trajectory $x(t)$. As we can see here, there are discontinuous changes of the slope because during this experiment the angle θ has been changed several times. For a better accuracy the velocity as a function of θ was obtained from a series of movies recorded at different angles θ . The results are plotted in Figure 3.14 a). Obviously there is a wide range of angles Φ , where $\Phi = \pi - \theta$, in which velocity is proportional to Φ . We noticed a linear behavior of $v(\Phi)$ in the vicinity of $\Phi = 0$, due to symmetry reasons represented in Figure 3.14 b). The scheme on the right represents the distortion of the director field in the presence of the magnetic field with $\Phi > 0$. When the field is strong enough the distortion is localized in a cylindrical shell whose thickness is given by the magnetic coherence length $\xi(\mathbf{B})$. The energy per unit length (in x direction) of this cylindrical shell can be seen as a force pulling on the disclination loop. Clearly, as the distortion on the left side of the disclination loop (labeled ∇) is larger than on its right side (labeled Δ), the resulting force drives the motion of the loop to the left as shown. Upon the reversal of the sign of the director field is transformed by reflection in the mirror orthogonal to the fiber and the sign of the loop's velocity v is reversed too.

Analytically, for this symmetry reason, in the expansion of $v(\Phi)$ into a Fourier series only sine terms $\sin(m\Phi)$ can occur. Moreover, as the distortion should not depend on the sign of \mathbf{B} must be pair so that finally one gets the expression:

$$v(\Phi) = a \sin(2\Phi) + b \sin(4\Phi) + \dots \quad (3.21)$$

which in the limit of small angles Φ leads to a linear dependence of v on Φ :

$$v = \frac{dx}{dt} \approx \alpha \Phi \quad (3.22)$$

Remarkably, the experimentally observed linear dependence of v on Φ (see Figure 3.14 a)) is not limited to the vicinity of $\Phi = 0$ but holds in a wide interval of angles $-60^\circ < \Phi < 60^\circ$.

The fit of this linear dependence to experimental results in Figure 3.14 a) leads to a positive coefficient α .

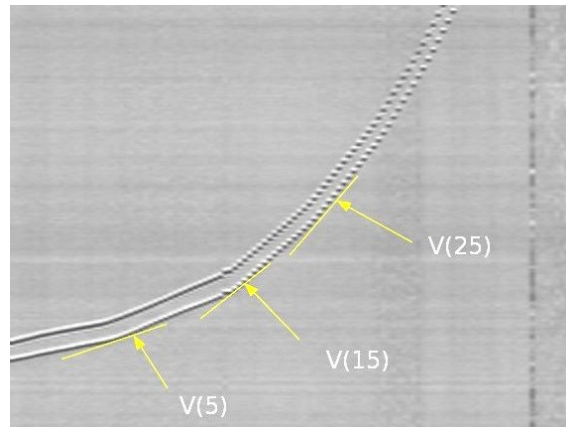


Figure 3.13: Reslice of the image sequence, showing the increasing of the velocity of the disclination loop, with the increasing of the field angle between the disclination loop and the magnets.

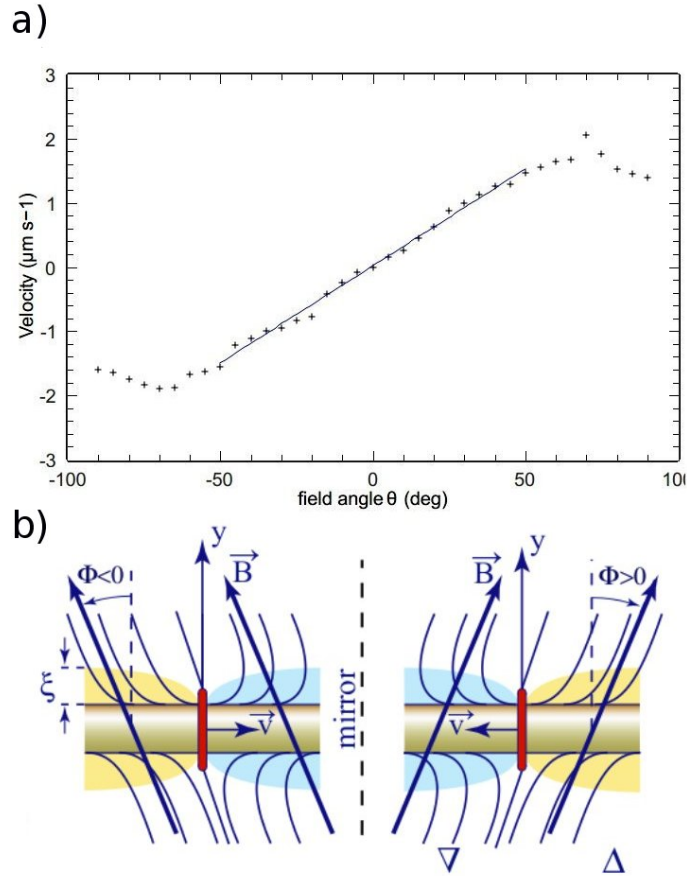


Figure 3.14: a) Plot of the velocity of the disclination loop versus the field angle θ ($\theta = \pi - \Phi$) between the fiber main axis and the horizontal homogeneous magnetic field created by the two magnets. The plain line in this graph represents the best linear fit to experimental results in the interval $[-50^\circ, 50^\circ]$; b) symmetry relationship explaining the odd dependence of v on Φ .

Let us emphasize that these results are in agreement with the theoretical analysis in sections 3.1, 3.2 and 3.3.

3.8 Horizontal magnetic fields on CA electrospinning fibers

As previously mentioned in section 2, the fibers used in this experiment were produced by electrospinning, which due to its importance must be detailed. The process begins with the placement of the syringe containing a polymeric solution on the pump. In our experiment we used a CA solution. The pump forces the solution to come out at a constant rate of 0.02 ml h^{-1} , and due to the application of an high potential to the nozzle (20 kV), a drop is formed. The charged drop is then deformed, presenting a conical shape called Taylor cone[36], and ejected toward the target, when the electrostatic forces are higher than the surface tension of the polymeric solution. This jet is steady in the region near the needle[37], traveling along a straight path. In the region near the target, the jet is more unstable, assuming a spiral path, when the electrostatic forces and the surface tension are equal[4, 32]. The distance between the nozzle and the target should be large enough to allow the evaporation of the solvent, to allow the formation of fibers instead of droplets. We used 15 cm in our experiment. The electrospinning setup used in the experiment, as

well as the target, can be observed in Figure 3.15 a) and Figure 3.15 b), respectively.

During the process is necessary to control not only the distance between the needle and the target, but also other critical parameters, such as the humidity and the temperature of the room, as well as the concentration and the viscosity of the polymeric solution[38].

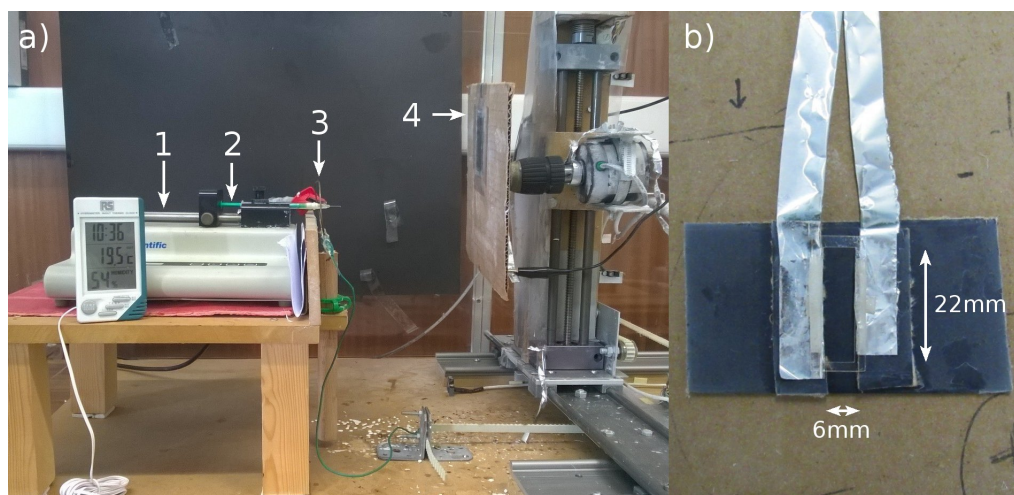


Figure 3.15: a) Photograph of the electrospinning setup: 1- infusion pump KDS100; 2- syringe; 3- coaxial shield ring; 4- target. The flow rate, the voltage used and the distance between the needle and the target were, respectively: 0.02 mlh^{-1} , 20 kV and 15 cm . b) Photograph of the target, where we can see the plastic frame, coated with double sided adhesive tape, glued on top of the aluminum stripes separated by 6 mm .

As already explained, the samples were prepared by overlapping two glass plates, previously treated with egg yolk, and the support with the suspended fibers was placed in the middle. To study the presence of disclination loops on these fibers, and their behavior when a horizontal and homogeneous magnetic field is applied, we used a different setup from the first two, illustrated in Figure 3.16. For this purpose, a regular polarized light microscope was used. First, without applying the magnetic field, the sample was simply placed in the microscope platinum, to see the presence of the disclination loops, and several pictures were taken with the following microscope lenses: 10x, 20x and 50x. The sample was observed using the transmission mode of the microscope. Some POM pictures are illustrated in Figure 3.17, where we can easily see the presence of these disclination loops.

To study the behavior of these disclination loops with the application of an horizontal and homogeneous magnetic field, the sample was placed on the microscope platinum first. Then, the magnet holder was placed on top of the sample, without being in contact with it. The angle between the fiber main axis and the magnets assumed the values of 0 and 90 degrees, controlled by the angles marked in the platinum. For each case we recorded sequences of images using the software QUALQUER COISA. This procedure was done in the liquid crystalline phase, at room temperature, but also in the isotropic phase, heating the sample using the heating/cooling stage. Due to the difficulty in handling all the components of the setup in such a small space, the heating stage was placed next to the microscope platinum, at the same high, and the heating was done using a copper strip. One side of the stripe was placed inside the heating/cooling stage, while the other side was glued on the top of the sample. To observe the sample we did a circumferential hole in the strip, with few millimeters in diameter. We programmed the heating for 250° C , and

the sample was heated by conduction. We used a high heating value due to the energy losses that occur due to the size of the strip.

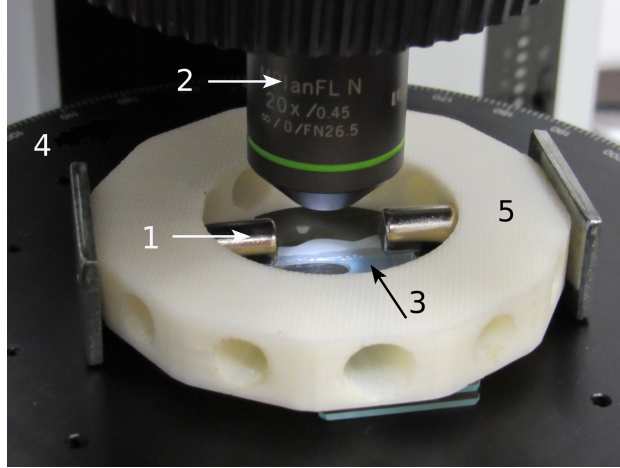


Figure 3.16: Photograph of the setup: 1- magnet; 2- microscope lens; 3- sample; 4- microscope platinum; 5- magnet holder. Electrospinning fibers inserted in a sample with homeotropic anchoring, and filled with the nematic liquid crystal 5CB, are submitted to an horizontal and homogeneous magnetic field, created by two cylindrical magnets. The angle between the fibers main axis and the magnets is controlled by the angles marked in the platinum. The microscope used is a polarized light microscope.

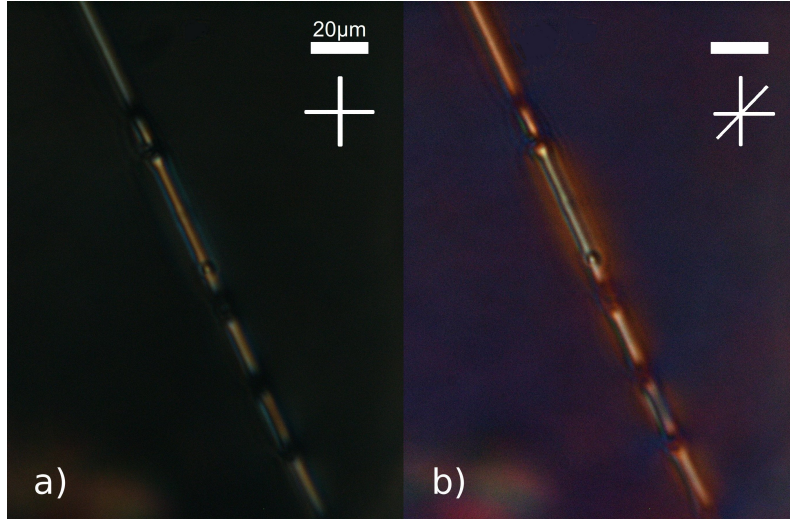


Figure 3.17: POM pictures of cellulose acetate fibers, produced from a CA solution (12%w/w), in a homeotropic sample: a) under crossed polarizers; b) between cross-polarizers with a 530nm retardation plate. The different colors surrounding the fiber, yellow and blue, show us that there are different orientation of the director field \vec{n} along the fiber[27]. The average diameter of the fibers is $4\mu m$. These fibers induce disclination loops which can be seen easily in these two photographs, that are perpendicular to the fiber main axis, due to the planar anchoring on the fiber surface and the homeotropic anchoring of the sample walls.

After applying the horizontal and homogeneous magnetic field to the sample, varying the angle θ , the image sequences recorded were analyzed using the software VLC media player. Unlike what happened in the last case, where the captive disclination loops threaded on nylon fibers moved

across the fiber with a velocity v , in this case the captive disclination loops remained in the same place, not showing any movement. This occurred in both phases, and for both values of θ . The cause for such an occurrence could be explained by the fiber diameter. In the case of the nylon fiber, the diameter was $200\mu m$ (see Figure 3.18). In this case, we have fibers of smaller dimensions, with approximately $4\mu m$, see Figure 3.17. This can indicate that there is a critical diameter from which the disclination loop does not move, due to the attraction force f_L (see Figure 3.18) that the fiber exerts on the disclination loop.

We also noticed that although the disclination loops did not move, the fibers showed slight fluctuations when the field was applied in the liquid crystalline phase and in the isotropic phase. The fact that they have moved in the isotropic phase shows us that the nematic liquid crystal does not interfere with the fiber movement, being only due to the action of the magnetic forces created by the two magnets[39].

In order to know the critical diameter from which the disclination loop doesn't vanish throughout the medium, it is necessary to do some calculations. It is known that there are two forces acting on a disclination loop, the Laplace force (f_L), 3.23, and f_r which is opposed to the first one, 3.24, respectively[4]:

$$f_L = \frac{T_e}{R+h} \quad (3.23)$$

$$f_r = 2\pi K \frac{m^2}{2h} \quad (3.24)$$

Where h is the distance between the fiber and the disclination; R is the fiber's diameter; K is the isotropic elasticity; m is the disclinations line strength and T_e is the disclinations line tension. The parameters h and R , as well as the two forces f_L and f_r are schematically represented in Figure 3.18.

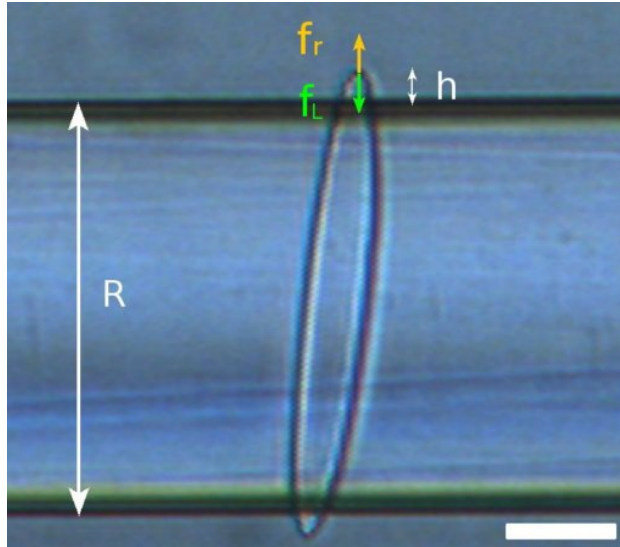


Figure 3.18: Picture a captive disclination loop on a nylon fiber, where the equilibrium distance h , as well as R , f_L and f_r are schematically represented. The scale bar corresponds to $50\mu m$.

Taking into account that the radius of the fiber is much larger than h ($R \gg h$), comes that:

$$f_L \approx \frac{T_e}{R} \quad (3.25)$$

Due to the fact that the disclination ring is in equilibrium and doesn't move across the fiber, it comes:

$$f_r = f_L = \frac{T_e}{R} = 2\pi K \frac{m^2}{2h} \quad (3.26)$$

Finally, and knowing that $m = +1/2$, the final expression to the equilibrium distance h is given by[6]:

$$h = R \frac{\pi K}{4T_e} \approx R \frac{K}{T_e} \quad (3.27)$$

3.9 Horizontal magnetic fields on natural fibers

After preparing the samples in the same way as the previous ones, they were observed also using a transmission mode microscope. The POM pictures are represented in Figure 3.19. The samples were also submitted to an horizontal and homogeneous magnetic field, using the same setup and conditions as already explained in section 3.7.

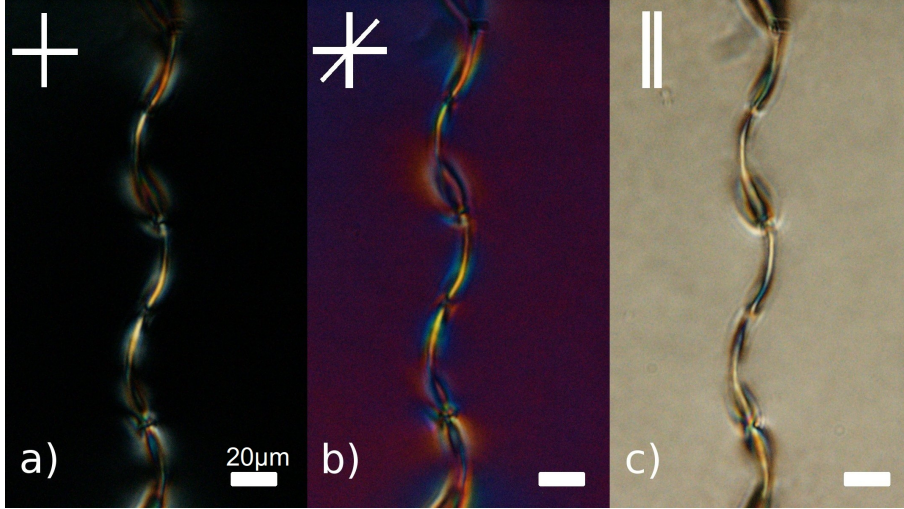


Figure 3.19: POM pictures of the natural fibers taken from the plant called *Ornithogalum thyrsoides*, in a homeotropic sample: a) under crossed polarizers; b) between cross-polarizers with a 530nm retardation plate; c) between parallel polarizers. We can easily see that these fibers also induce disclination loops. Through a close observation of the picture b), we noticed that the direction of the nematic molecules in the regions near the disclination loops varies. This could be seen by the change of colors between yellow and blue[27]. The average diameter of the fibers is $2\mu m$.

In a first analysis, we can say that these disclination loops do not exist only in synthetic fibers, like the previous ones, but also in fibers extracted from natural plants.

After applying the horizontal and homogeneous magnetic field to the sample, giving θ the same values of 0 and 90 degrees, the results were very similar to the ones using CA electrospinning fibers. Due to the small diameter of the fibers, the disclination loops are strongly attracted to the fiber, like we explained in section 3.8, causing them not to move when we applied the horizontal

and homogeneous magnetic field. The main difference to the CA and nylon fibers is that these fibers have a pronounced curvature, which is not the case of the last two. This shows us that the movement of the disclination loops with the application of the magnetic field is not related to the curvature of the fibers, but with their diameter.

Conclusions and Future Perspectives

While topological defects should be avoided in nematic liquid crystal electro-optical sensors and displays this work demonstrates that 1D defects, i.e. disclination lines, can have some use if precisely designed and manipulated. In particular, it is possible to generate the so-called captive disclination loops threaded on fibers immersed in nematic cells.

It has been pointed out that such captive disclination loops can be manipulated, i.e. translated and tilted, by electric and magnetic fields.

Tilting captive disclination loops in electric or magnetic fields was found to be a source of information about the fibers morphologies. Indeed, the field-induced tilt of a disclination loop with respect to the fiber axis is correlated with the fibers' chirality (for fibers with diameters ranging from hundred to few micrometers).

Captive disclination loops have also been put in a translational motion by the action of a magnetic field oblique to fibers and their velocities were found to vary as a function of the field intensity and orientation as well as of the fibers' diameters. While velocities of $2\mu\text{m s}^{-1}$ were achieved for rings moving along fibers with diameters of $200\mu\text{m}$ driven by the action of an oblique magnetic field, no motion was observed, using the same drive driving conditions, if fibers with diameters of the order of $1 - 1.5\mu\text{m}$ were used. A reason for this behavior was given considering the disclination tension line, which is highly dependent on the radius of the fiber: $h = R \frac{\pi K}{4T_e}$.

For the future, new interactive technology for transport of living matter can be foreseen using systems of captive disclination loops generated on fibers' networks with special geometries immersed in nematic liquid crystalline cells.

- [1] X. Wang, Y.-K. Kim, E. Bukusoglu, B. Zhang, D. S. Miller, and N. L. Abbott. “Experimental Insights into the Nanostructure of the Cores of Topological Defects in Liquid Crystals”. In: *Physical review letters* 116.14 (2016), p. 147801.
- [2] X. Wang, D. S. Miller, E. Bukusoglu, J. J. de Pablo, and N. L. Abbott. “Topological defects in liquid crystals as templates for molecular self-assembly”. In: *Nature materials* 15.1 (2016), pp. 106–112.
- [3] F. J. Antonio. “Estudo de Defeitos Topológicos em Cristais Líquidos do Ponto de Vista Cosmológico”. Master’s Thesis. Universidade Estadual de Maringá, 2009, p. 121.
- [4] P. Pieranski, Pawel, Oswald. *Nematic and Cholesteric Liquid Crystals*. Taylor & Francis, 2005, p. 616.
- [5] M. Cardoso. “Contribuição para o Estudo da Fase Nemática Biaxial em Dendrímeros Líquido-Cristalinos Termotrópicos”. Master’s Thesis. Instituto Superior Técnico, 2007, p. 68.
- [6] A. de Oliveira. “Cellulose micro/nano fibers conformational effects probed by nematic liquid crystal droplets”. Master’s Thesis. FCT, 2014, p. 38.
- [7] A. Sengupta. *Topological microfluidics: nematic liquid crystals and nematic colloids in microfluidic environment*. Springer Science & Business Media, 2013.
- [8] J. de Gennes and J Prost. *The physics of liquid crystals*. 83. Oxford University Press, 1995.
- [9] S. Čopar. “Topology and geometry of nematic braids”. In: *Physics Reports* 538.1 (2014), pp. 1–37.
- [10] G. Volovik and O. Lavrentovich. “Topological dynamics of defects: boojums in nematic drops”. In: *Zh Eksp Teor Fiz* 85.6 (1983), pp. 1997–2010.
- [11] D. D. Luders. “Estudo de propriedades ópticas de uma fase nemática calamítica”. PhD Thesis. Universidade Estadual de Maringá, 2014, p. 123.
- [12] D. Andrienko. “Introduction to liquid crystals”. In: *IMPRS school, Bad Marienberg* (2006).
- [13] R. A. Alla. “On the Control of Nematic Liquid Crystal Alignment”. PhD Thesis. University of Gothenburg, 2013, p. 49.
- [14] F. C. Frank. “I. Liquid crystals. On the theory of liquid crystals”. In: *Discussions of the Faraday Society* 25 (1958), pp. 19–28.
- [15] C. M. Tone, M. P. De Santo, M. G. Buonomenna, G. Golemme, and F. Ciuchi. “Dynamical homeotropic and planar alignments of chromonic liquid crystals”. In: *Soft Matter* 8.32 (2012), pp. 8478–8482.
- [16] C. Tone, M. De Santo, and F Ciuchi. “Alignment of chromonic liquid crystals: A difficult task”. In: *Molecular Crystals and Liquid Crystals* 576.1 (2013), pp. 2–7.

-
- [17] T. Lubensky, D. Pettey, N. Currier, and H. Stark. “Topological defects and interactions in nematic emulsions”. In: *Physical Review E* 57.1 (1998), p. 610.
- [18] M. Kleman and O. D. Lavrentovich. “Topological point defects in nematic liquid crystals”. In: *Philosophical Magazine* 86.25-26 (2006), pp. 4117–4137.
- [19] J. Nehring and A. Saupe. “On the schlieren texture in nematic and smectic liquid crystals”. In: *Journal of the Chemical Society, Faraday Transactions 2: Molecular and Chemical Physics* 68 (1972), pp. 1–15.
- [20] J. de Gennes. “Nematic Liquid Crystals: Defects”. In: I (1993), pp. 1–5.
- [21] O. Lavrentovich. “Defects in liquid crystals: surface and interfacial anchoring effects”. In: *Patterns of Symmetry Breaking*. Springer, 2003, pp. 161–195.
- [22] G. Vertogen and W. H. de Jeu. *Thermotropic liquid crystals, fundamentals*. Vol. 45. Springer Science & Business Media, 2012.
- [23] O. D. Lavrentovich and E. M. Terentjev. “Phase transition altering the symmetry of topological point defects (hedgehogs) in a nematic liquid crystal”. In: *Soviet Physics JETP* 64.December 1986 (1986), pp. 1237–1244.
- [24] Y.-S. Wang, B.-H. Yuan, and G.-H. Yang. “Effect of Saddle-Splay Elasticity on Stability of Disclination Rings in Nematic Liquid Crystals”. In: *Communications in Theoretical Physics* 50.4 (2008), pp. 847–850.
- [25] G. P. Alexander, B. G. G. Chen, E. A. Matsumoto, and R. D. Kamien. “Colloquium: Disclination loops, point defects, and all that in nematic liquid crystals”. In: *Reviews of Modern Physics* 84.2 (2012), pp. 497–514.
- [26] Y Geng, D Seč, P. L. Almeida, O. D. Lavrentovich, S Žumer, and M. H. Godinho. “Liquid crystal necklaces: Cholesteric drops threaded by thin cellulose fibres”. In: *Soft Matter* 9.33 (2013), pp. 7928–7933.
- [27] S. Čopar, D. Seč, L. E. Aguirre, P. L. Almeida, M. Dazza, M. Ravnik, M. H. Godinho, P. Pieranski, and S. Žumer. “Sensing and tuning microfiber chirality with nematic chirogyral effect”. In: *Physical Review E* 93.3 (2016), p. 032703.
- [28] B. J. Frisken. “Nematic liquid crystals in electric and magnetic fields”. PhD thesis. University of British Columbia, 1989.
- [29] M. S. Roh, A. K. Lee, and J. K. Suh. “Induction of bulb maturity of *Ornithogalum thyrsoides*”. In: *Scientia horticultruae* 114.2 (2007), pp. 138–141.
- [30] M. Nikkhou, M. Škarabot, S. Čopar, M. Ravnik, S. Žumer, and I. Mušević. “Light-controlled topological charge in a nematic liquid crystal”. In: *Nature physics* 11.2 (2015), pp. 183–187.
- [31] Y. Geng, P. L. Almeida, J. L. Figueirinhas, E. M. Terentjev, and M. H. Godinho. “Liquid crystal beads constrained on thin cellulosic fibers: electric field induced microrotors and N–I transition”. In: *Soft Matter* 8.13 (2012), pp. 3634–3640.
- [32] M. Nikkhou, M. Škarabot, S. Čopar, M. Ravnik, S. Žumer, and I. Mušević. “Light-controlled topological charge in a nematic liquid crystal”. In: *Nature physics* 11.2 (2015), pp. 183–187.
- [33] M Nikkhou, M Škarabot, and I Mušević. “Topological binding and elastic interactions of microspheres and fibres in a nematic liquid crystal”. In: *The European Physical Journal E* 38.3 (2015), pp. 1–15.

- [34] L. E. Aguirre, A. de Oliveira, D. Seč, S. Čopar, P. L. Almeida, M. Ravnik, M. H. Godinho, and S. Žumer. “Sensing surface morphology of biofibers by decorating spider silk and cellulosic filaments with nematic microdroplets”. In: *Proceedings of the National Academy of Sciences* 113.5 (2016), pp. 1174–1179.
- [35] K. A. Takeuchi and M. Sano. “Universal fluctuations of growing interfaces: evidence in turbulent liquid crystals”. In: *Physical review letters* 104.23 (2010), p. 230601.
- [36] E. Jentsch, Ö. Gül, and E. Öznergiz. “A comprehensive electric field analysis of a multifunctional electrospinning platform”. In: *Journal of Electrostatics* 71.3 (2013), pp. 294–298.
- [37] S. Ramakrishna, K. Fujihara, W.-E. Teo, T.-C. Lim, and Z. Ma. *An introduction to electrospinning and nanofibers*. Vol. 90. World Scientific, 2005.
- [38] L. G. Soares. “Obtenção por electrospinning e caracterização de fibras nanoestruturadas de TiO₂ e sua aplicação fotocatalítica”. In: (2013).
- [39] C Lapointe, A Hultgren, D. Silevitch, E. Felton, D. Reich, and R. Leheny. “Elastic torque and the levitation of metal wires by a nematic liquid crystal”. In: *Science* 303.5658 (2004), pp. 652–655.

Taking into account the Figure 3.1, the orientation of the molecules \vec{n} in the transition layer is given by:

$$n_x = \sin \beta(y); n_y = 0; n_z = \cos \beta(y)$$

The magnetic field \vec{B} is given by:

$$B_x = B; B_y = 0; B_z = 0$$

. Using the Frank energy density equation:

$$F_d = \frac{1}{2}K_{11}(\text{div } \vec{n})^2 + \frac{1}{2}K_{22}(\vec{n} \cdot \text{rot } \vec{n})^2 + \frac{1}{2}K_{33}(\vec{n} \times \text{rot } \vec{n})^2 - \frac{1}{2}\varepsilon_0\varepsilon_a(\vec{n} \cdot \vec{B})^2 \quad (\text{A.1})$$

Where $-\frac{1}{2}\varepsilon_0\varepsilon_a(\vec{n} \cdot \vec{B})^2$ is the magnetic field component.

To resolve the equation it is necessary to do some calculations first:

$$\text{div } \vec{n} = \frac{\partial n_x}{\partial x} + \frac{\partial n_y}{\partial y} + \frac{\partial n_z}{\partial z} = 0$$

$$\text{rot } \vec{n} = \begin{vmatrix} \vec{e}_1 & \vec{e}_2 & \vec{e}_3 \\ \frac{\partial}{\partial x} & \frac{\partial}{\partial y} & \frac{\partial}{\partial z} \\ n_x & 0 & n_z \end{vmatrix} = \vec{e}_1 \left(\frac{\partial n_z}{\partial y} \right) + \vec{e}_3 \left(-\frac{\partial n_x}{\partial y} \right)$$

$$\begin{aligned} \vec{n} \cdot \text{rot } \vec{n} &= (n_x \vec{e}_1 + n_z \vec{e}_3) \cdot \left[\left(\frac{\partial n_z}{\partial y} \right) \vec{e}_1 - \left(\frac{\partial n_x}{\partial y} \right) \vec{e}_3 \right] = n_x \frac{\partial n_z}{\partial y} - n_z \frac{\partial n_x}{\partial y} = \\ &= \sin \beta \frac{\partial \cos \beta}{\partial \beta} \frac{\partial \beta}{\partial y} - \cos \beta \frac{\partial \sin \beta}{\partial \beta} \frac{\partial \beta}{\partial y} = -\sin \beta^2 \frac{\partial \beta}{\partial y} - \cos \beta^2 \frac{\partial \beta}{\partial y} = \left(-\frac{\partial \beta}{\partial y} \right) \end{aligned}$$

$$(\vec{n} \cdot \text{rot } \vec{n})^2 = \left(\frac{\partial \beta}{\partial y} \right)^2$$

$$\vec{n} \times \text{rot } \vec{n} = \begin{vmatrix} \vec{e}_1 & \vec{e}_2 & \vec{e}_3 \\ n_x & 0 & n_z \\ \frac{\partial n_z}{\partial y} & 0 & -\frac{\partial n_x}{\partial y} \end{vmatrix} = -\vec{e}_2 \left(-n_x \frac{\partial n_x}{\partial y} - n_z \frac{\partial n_z}{\partial y} \right) =$$

$$= n_x \frac{\partial n_x}{\partial \beta} \frac{\partial \beta}{\partial y} - n_z \frac{\partial n_z}{\partial \beta} \frac{\partial \beta}{\partial y} = -\sin \beta \cos \beta \frac{\partial \beta}{\partial y} + \cos \beta \sin \beta \frac{\partial \beta}{\partial y} = 0$$

$$\vec{n} \cdot \vec{B} = (\sin \beta \vec{e}_1 + \cos \beta \vec{e}_3) \cdot (B_x \vec{e}_1 + B_y \vec{e}_2 + B_z \vec{e}_3) = B \sin \beta$$

$$(\vec{n} \cdot \vec{B})^2 = B^2 \sin^2 \beta$$

replacing in the equation A.1:

$$F_d = \frac{1}{2} K_{22} \left(\frac{\partial \beta}{\partial y} \right)^2 - \frac{1}{2} \chi_a B^2 \sin^2 \beta \quad (\text{A.2})$$

Where $\chi_a = \chi_{||} - \chi_{\perp}$

Taking into account the minimum condition:

$$-\frac{\partial f_d}{\partial n_i} + \frac{d}{dn_j} \frac{\partial f_d}{\partial n_{i,j}}$$

We have:

$$\begin{aligned} \frac{\partial}{\partial n_x} \left(\frac{1}{2} \chi_a B^2 \sin \beta \right) &= \chi_a B^2 \cos \beta \sin \beta \\ \frac{d}{dy} \left(\frac{\frac{1}{2} K_{22} \left(\frac{\partial \beta}{\partial y} \right)^2}{\partial \left(\frac{\partial \beta}{\partial y} \right)} \right) &= K_{22} \frac{\partial^2 \beta}{\partial y^2} \end{aligned}$$

Coming to the equation A.3:

$$K_{22} \frac{\partial^2 \beta}{\partial y^2} + \chi_a B^2 \cos \beta \sin \beta = 0 \quad (\text{A.3})$$

Considering now the equation A.4:

$$\xi(B) = \frac{\left(\frac{K_{22}}{\chi_a} \right)^{1/2}}{B} \quad (\text{A.4})$$

Where $\xi(B)$ is the persistence length.

replacing in the equation A.4 it comes:

$$\xi^2 \frac{\partial^2 \beta}{\partial y^2} + \sin \beta \cos \beta = 0$$

This must be integrated. For that reason, we use a simple trick of multiplying the last equation by $d\beta/dy$:

$$\frac{d\beta}{dy} \xi^2 \frac{d^2\beta}{dy^2} + \frac{d\beta}{dy} \sin\beta \cos\beta = 0$$

$$\frac{d}{dy} \left[\xi^2 \frac{1}{2} \left(\frac{d\beta}{dy} \right)^2 \right] + \frac{d}{dy} \left(-\frac{1}{2} \cos^2 \beta \right) = 0$$

Because:

$$\frac{d}{dy} \left[\frac{1}{2} \left(\frac{d\beta}{dy} \right)^2 \right] = 2 \times \frac{1}{2} \frac{d\beta}{dy} \frac{d^2\beta}{dy^2} = \frac{d\beta}{dy} \frac{d^2\beta}{dy^2}$$

and

$$\frac{d}{dy} \left(-\frac{1}{2} \cos^2 \beta \right) = -\frac{1}{2} \times 2 \cos \beta (-\sin\beta) \frac{d\beta}{dy} = \cos \beta \sin \beta \frac{d\beta}{dy}$$

So we have:

$$\begin{aligned} \frac{d}{dy} \left[\xi^2 \frac{1}{2} \left(\frac{d\beta}{dy} \right)^2 - \frac{1}{2} \cos^2 \beta \right] &= 0 \\ \xi^2 \frac{1}{2} \left(\frac{d\beta}{dy} \right)^2 - \frac{1}{2} \cos^2 \beta &= c \end{aligned}$$

So we have:

$$\xi^2 \left(\frac{d\beta}{dy} \right)^2 = \cos^2 \beta + c$$

Far from the wall, the conditions are: $y \rightarrow \infty$, $\beta = \pi/2$ and $d\beta/dy = 0$, being $c = 0$.

Therefore:

$$\begin{aligned} \xi^2 \left(\frac{d\beta}{dy} \right)^2 &= \cos^2 \beta \\ \xi \frac{d\beta}{dy} &= \pm \cos \beta \end{aligned}$$

Where both options are possible, due to the possibility of rotating to both sides.

Considering the positive sign:

$$\begin{aligned} \xi \frac{d\beta}{dy} &= \cos \beta \\ \frac{dy}{\xi} &= \frac{d\beta}{\cos \beta} \end{aligned}$$

If:

$$u = \frac{\pi}{2} - \beta \Rightarrow \frac{dy}{\xi} = \frac{d\beta}{\cos \beta} = -\frac{du}{\sin u}$$

To resolve the equation, we have to do a change of variable:

$$t = \tan(u/z)$$

Getting:

$$\sin u = \frac{2t}{1+t^2}$$

and

$$du = \frac{2dt}{1+t^2}$$

So we get that:

$$\frac{dy}{\xi} = \frac{\frac{-2dt}{(1+t^2)}}{\frac{2t}{(1+t^2)}} = -\frac{dt}{t}$$

$$\frac{dy}{\xi} = -\frac{dt}{t} \Rightarrow \ln(t) = -\frac{y}{\xi} + c_1$$

$$t = \exp\left(-\frac{y}{\xi} + c_1\right) = c_2 \exp\left(-\frac{y}{\xi}\right)$$

The conditions near the wall are: $y = 0$ and $\beta = 0$

So we have:

$$u = \frac{\pi}{2}$$

$$t = \tan\left(\frac{\pi}{4}\right) = 1$$

$$1 = c_2 \exp(0) = c_2 \rightarrow c_2 = 1$$

Therefore:

$$t = \exp\left(\frac{y}{\xi}\right) \equiv \operatorname{tg}\left(\frac{(\pi/2) - \beta}{2}\right) = \exp\left(-\frac{y}{\xi}\right)$$

Where ξ is the magnetic coherence length.

Considering:

$$t = \exp\left(\frac{y}{\xi}\right)$$

and

$$\xi(B) = \frac{\left(\frac{K_{22}}{\chi_a}\right)^{1/2}}{B}$$

And replacing with $K_{22} = 10^{-6}$; $\chi_a = 10^{-7}$ and $B = 10^4$ (SI), we can calculate:

$$\xi(B) = 3\mu m$$

With a very weak external perturbation, we can induce distortions on a scale comparable to an optical wave-length.